

1 **Biotic Response of Plankton Communities to Middle to Late**  
2 **Miocene Monsoon Wind and Nutrient Flux Changes in the**  
3 **Oman Margin Upwelling Zone**

4 Gerald Auer<sup>1</sup>, Or M. Bialik<sup>2,3</sup>, Mary-Elizabeth Antoulas<sup>1</sup>, Noam Vogt-Vincent<sup>4</sup>, Werner E.  
5 Piller<sup>1</sup>

6 <sup>1</sup>University of Graz, ~~Institute-Department~~ of Earth Sciences, NAWI Graz Geocenter, Heinrichstrasse 26, 8010  
7 Graz, Austria

8 <sup>2</sup>~~University of Muenster~~, Institute of Geology and Palaeontology, ~~University of Muenster~~, Corrensstr. 24, 48149  
9 Münster, Germany

10 <sup>3</sup>Dr. Moses Strauss Department of Marine Geosciences, The Leon H. Charney School of Marine Sciences,  
11 University of Haifa, Carmel 31905, Israel.

12 <sup>4</sup>Department of Earth Sciences, University of Oxford, Oxford, UK

13 *Correspondence to: Gerald Auer (gerald.auer@uni-graz.at) & Or M. Bialik (obialik@uni-muenster.de)*

14  
15 **Keywords**

16 Indian summer monsoon, upwelling, Miocene, calcareous nannoplankton, intermediate waters, nutrient fluxes

17

18

19 **Abstract.** ~~Understanding past dynamics the behaviour of past upwelling cells is an important aspect of assessing~~  
20 ~~potential upwelling changes in future climate change scenarios.~~ Our present understanding of nutrient fluxes  
21 throughout the world's oceans emphasizes the importance of intermediate waters transporting nutrients from the  
22 Antarctic divergence into the middle and lower latitudes. These nutrient-rich waters fuel productivity within wind-  
23 driven upwelling cells in all major oceans. One such upwelling ~~cell-system~~ is located along the Oman Margin in  
24 the Western Arabian Sea (WAS). Driven by cross-hemispherical winds, the WAS upwelling zone's intense  
25 productivity led to the formation of one of the most extensive oxygen minimum zones known today.

26 In this study covering the Middle to Late Miocene at ODP Site 722, we investigate the inception of upwelling-  
27 derived primary productivity. ~~We-This study presentseombine novel dataanew plankton assemblage data in the~~  
28 ~~context of existingwith-existing~~ model- and data-based evidence ~~,-constrainingeonstraining-~~ the tectonic and  
29 atmospheric boundary conditions for ~~an upwelling cellupwelling in the WAS~~to exist in the region. With this  
30 research, we build upon the original planktonic foraminifer-based research by Dick Kroon in 1991 as part of his  
31 research based on the Ocean Drilling Project (ODP) LEG 117.

32 We show that monsoonal winds likely sustained upwelling since the emergence of the Arabian Peninsula after the  
33 Miocene Climatic Optimum (MCO) ~14.7 Ma, with fully monsoonal conditions occurring since the end of the  
34 Middle Miocene Climatic Transition (MMCT) ~13 Ma. However, changing nutrient fluxes through Antarctic  
35 Intermediate and sub-Antarctic Mode Waters (AAIW/SAMW) were only established ~~by-after~~ ~12 Ma. Rare  
36 occurrences of diatoms frustules correspond to the maximum abundances of *Reticulofenestra haqii* and  
37 *Reticulofenestra antarctica*, indicating higher upwelling-derived nutrient levels. By 11 Ma, diatom abundance  
38 increases significantly, leading to alternating diatom blooms and high-nutrient-adapted nannoplankton taxa. These  
39 changes in primary producers are also well reflected in geochemical proxies with increasing  $\delta^{15}\text{N}_{\text{org}}$  values (> 6‰)  
40 and high organic carbon accumulation. ~~also-These proxies provide further independent evidence for eonfirm~~ high  
41 productivity and ~~beginning the onset of~~ denitrification simultaneously.

42 ~~Our multi-proxy based evaluation of Site 722 primary producers provides evidence for a stepwise evolution of~~  
43 ~~Middle to Late Miocene productivity in the western Arabian Sea for the first time. The absence of full~~  
44 ~~correspondence withof a clear correlation with-existing deep marine climate records also suggests that local~~  
45 ~~processes, such as monsoonal wind conditions but crucially also lateral nutrient transport through upwelling~~  
46 ~~intermediate waters, likely played an important role in modulating productivity in the western Arabian Sea. Finally,~~  
47 ~~we show that using a multi-proxy record provides novel insights into how fossil plankton responded to changing~~  
48 ~~nutrient conditions through time in a monsoon wind-driven upwelling zone.~~

49 ~~Our multi-proxy-based evaluation of Site 722 primary producers provides evidence for a stepwise evolution of~~  
50 ~~Middle to Late Miocene productivity in the western Arabian Sea for the first time. The absence of a clear~~  
51 ~~correlation with existing deep marine climate records also suggests that local processes, such as monsoonal wind~~  
52 ~~conditions but crucially also hints at changing lateral nutrient transport through upwelling intermediate waters,~~  
53 ~~likely played an important role in modulating productivity in the western Arabian Sea. Finally, we show that using~~  
54 ~~a multi-proxy record provides novel insights into how plankton responded to changing nutrient conditions through~~  
55 ~~time in a monsoon-wind-driven upwelling zone.~~

56 **1. Introduction**

57 Within coastal upwelling zones, wind-driven Ekman transport brings nutrient-rich deep water into the photic zone  
58 (Woodward et al., 1999). This process supports enhanced primary productivity in the surface ocean. This increased  
59 productivity supports a large biomass across the entire food chain, reaching far afield from the core of the  
60 upwelling zone. In addition, the high productivity in upwelling zones produces a significant amount of marine  
61 snow (both organic and inorganic), which sinks through the water column. As the organic particulates fall, they  
62 become partially remineralized, consuming oxygen and forming an oxygen-depleted zone. ~~At present the Arabian~~  
63 ~~Sea OMZ extends southwards from the Oman Margin between 200 and 1000 m water depth, reaching as far south~~  
64 ~~as 10°N~~ (Morrison et al., 1998; McCreary et al., 2013). ~~Yet~~ However, the flux of organic matter is so large that a  
65 significant volume of organic ~~matter and inorganic material~~ reaches and accumulates on the seafloor (e.g., Suess,  
66 1980; Rixen et al., 2019a, b).

67 Upwelling zones affect the marine carbon cycle by sequestering carbon and exchanging carbon between the ocean  
68 and the atmosphere via the dissolved inorganic carbon system and pCO<sub>2</sub> changes (Rixen et al., 2006; Krapivin and  
69 Varotsos, 2016; Wang et al., 2015). ~~During upwelling,~~ increased photosynthesis-driven primary productivity  
70 during upwelling results in produces high organic carbon export from the photic zone into the deep sea through the  
71 organic carbon pump (Volk and Hoffert, 1985; Ridgwell and Zeebe, 2005). Primary producers account for most  
72 of the biomass in upwelling zones, with phytoplankton accounting for > 80% of the particulate organic carbon  
73 (Head et al., 1996). Calcification by these primary producers and heterotrophic organisms feeding on them is  
74 further an important contributor to the inorganic carbon cycle of the oceans (Falkowski, 1997; Raven and  
75 Falkowski, 1999; Ridgwell and Zeebe, 2005; Millero, 2007).

76 However, the productivity of coastal upwelling zones highly depends on atmospheric conditions as they are  
77 primarily wind-driven. ~~Therefore~~ Consequently, wind-driven upwelling further constitutes a direct intersection  
78 between the oceans and the atmosphere. ~~Consequently~~ Hence, atmospheric changes in average wind speeds are  
79 directly responsible for the intensity and size of upwelling zones (Dugdale, 1972; Shimmield, 1992; Tudhope  
80 et al., 1996; Balun et al., 2010). Therefore, these atmospheric processes may also influence the community structure  
81 of primary producers and consumers within the area affected by upwelling.

82  
83 ~~In the Arabian Sea — one of the most productive marine regions today~~ (Lee et al., 1998; Honjo et al., 1999; Munz  
84 et al., 2017; Rixen et al., 2019b) oday, the Western Arabian Sea (WAS) upwelling is one of the most productive  
85 marine regions (Lee et al., 1998; Honjo et al., 1999; Munz et al., 2017; Rixen et al., 2019b). Its high productivity  
86 and organic matter flux fuels the Arabian Sea oxygen minimum zone (OMZ), which extends southwards from the  
87 Oman Margin between 200 and 1000 m water depth, reaching as far south as 10°N (Morrison et al., 1998;  
88 McCreary et al., 2013), making it one of the largest oxygen deficient zones in the modern ocean.  
89 Primary productivity in the WAS is furthermore is primarily driven by ~~the Indian Summer Monsoon (ISM)~~ seasonal  
90 winds flowing norward along the east coast of Africa in the northwestern Indian Ocean (Currie et al., 1973; Rixen  
91 et al., 2019a) as an extension of the Somali/Findlater Jets (Sarr et al., 2022; Findlater, 1969). Upwelling in the  
92 WAS the Western Arabian Sea (WAS) is thus directly forced by ~~this the~~ cross-hemispheric circulation system of  
93 the Indian Summer Monsoon (Findlater, 1969; Woodward et al., 1999; Basavani, 2013; Sarr et al., 2022). The  
94 prevailing southwesterly winds in the region during the summer months result in the displacement of large water  
95 masses (Tudhope et al., 1996; Schott and McCreary, 2001; Schott et al., 2009; Lahiri and Vissa, 2022), resulting  
96 in pronounced, intense upwelling peaks during the summer monsoon season (Lee et al., 1998; Honjo et al., 1999;

97 Rixen et al., 2019b). During the northern hemisphere winter, the prevailing wind direction in the Arabian Sea  
98 reverses as a weaker and dryer winter monsoon becomes established (Gadgil, 2018). The northeasterly winter  
99 monsoon winds result in an additional, albeit less pronounced, productivity spike in the region (Madhupratap et  
100 al., 1996; Munz et al., 2015, 2017; Rixen et al., 2019b). Between these two regimes – the inter-monsoon season –  
101 weak and variable winds dominate, permitting the establishment of well-stratified regions in the WAS that exhibit  
102 oligotrophic surface water conditions. ~~The shift between the different conditions generates a complex pattern of~~  
103 ~~abundance shifts between nutrient-adapted and primarily meso- but potentially even oligotrophic phytoplankton~~  
104 ~~communities. The~~ This dynamic impact of changes in wind regimes and upwelling intensity on plankton  
105 communities in the WAS is well-established for the modern (Schiebel et al., 2004). ~~The shift between the different~~  
106 ~~conditions generates a complex pattern of abundance shifts between nutrient-adapted and primarily meso- but~~  
107 ~~potentially even oligotrophic phytoplankton communities.~~  
108 In the Arabian Sea, significant variability in productivity has been identified over Pleistocene glacial-interglacials.  
109 For example, higher productivity in the Late Pleistocene is associated with interglacial periods (Schubert et al.,  
110 1998; Pourmand et al., 2007; Avinash et al., 2015; Naik et al., 2017). Conversely, these climatically driven changes  
111 in primary productivity affect the volume of the oxygen minimum zone (OMZ) and the intensity of denitrification  
112 in the region (Gaye et al., 2018). An OMZ is the result of the complete consumption of dissolved in the water  
113 column due to the microbial degradation of sinking organic matter. Hence OMZ strength is generally related to  
114 the strength of primary productivity and, thus, organic matter flux within the overlying upwelling cell (Dickens  
115 and Owen, 1994; McCreary et al., 2013; Stramma et al., 2008)  
116 Based on current records, the earliest activity within the upwelling zone may have already occurred earlier in the  
117 Burdigalian (Bialik et al., 2020b). However, it was not until connectivity to the proto-Mediterranean was  
118 terminated, and the Arabian Peninsula began to emerge that the regional geographic configuration allowed the  
119 establishment of a strong upwelling cell driven by the Findlater Jets (Rögl, 1999; Reuter et al., 2013; Harzhauser  
120 et al., 2007; Bialik et al., 2019; Sarr et al., 2022). After the Miocene Climatic Optimum (MCO) ~14 Ma (Flower  
121 and Kennett, 1994; Frigola et al., 2018; Sosdian and Lear, 2020), global cooling resumed, and a stable, upwelling  
122 zone and a sustained OMZ resembling present-present-day conditions was were reported to have established in the  
123 Western Indian Ocean WAS (Kroon et al., 1991; Zhuang et al., 2017; Bialik et al., 2020a).  
124 ~~This initiation of the upwelling occurred in conjunction with the intensification of the South Asian Monsoon~~  
125 ~~system (Gupta et al., 2015; Betzler et al., 2016).~~ Modelling studies suggest that the inception of upwelling and the  
126 monsoonal wind system WAS was closely linked to the tectonic evolution of the Arabian Peninsula, which resulted  
127 in water displacement by the Findlater Jet along a newly emergent coastline of Oman (Zhang et al., 2014; Sarr et  
128 al., 2022). Therefore, the uplift of the Arabian Peninsula is now seen as the dominant controlling factor for the  
129 inception of monsoonal upwelling in the WAS, which is now also seen as largely separate from prevailing  
130 monsoonal rainfall patterns (Sarr et al., 2022). After the tectonic configuration of the Arabian Peninsula was in  
131 place, the cross-hemispheric wind patterns of the South Asian Monsoon were subsequently able to drive upwelling  
132 in the WAS in a near modern configuration since the MMCT. ~~This initiation of the upwelling occurred in~~  
133 ~~conjunction with the intensification of the South Asian Monsoon system (Bialik et al., 2020a; Betzler et al., 2016;~~  
134 ~~Gupta et al., 2015).~~  
135  
136

137 Evidence suggests that strong upwelling in the Arabian Sea first occurred between the Middle and Late Miocene  
138 (Kroon et al., 1991; Huang et al., 2007a; Tripathi et al., 2017; Zhuang et al., 2017; Bialik et al., 2020a; Alam et  
139 al., 2022). To date, manganese redirection – i.e., the depletion of Mn in the sedimentary record due to Mn-reduction  
140 in the water column and subsequent advective transport to the edges of the OMZ – is one of the most used proxies  
141 to define OMZs and their past extent within the ocean (Dickens and Owen, 1994). Together with sedimentological  
142 facies and micropaleontological studies (Dickens and Owen, 1999; Gupta et al., 2004) these methods have been  
143 used most-effectively to track the size of the OMZ throughout the Indian Ocean and, by proxy, also the intensity  
144 of upwelling derived primary productivity.  $\delta^{15}\text{N}$  values  $> 6\%$  are seen as possible indicators for significant water  
145 column denitrification within the OMZ based on the approach of Tripathi et al. (2017). Bialik et al. (2020a) applied  
146 this approach for a Middle to Late Miocene interval at Site 722, showing that upwelling in the WAS may have  
147 sustained an OMZ strong enough for denitrification to occur as early as 11 Ma ago. However, these methods do  
148 not provide direct evidence for how changing wind and nutrient levels have interacted to result in the observed  
149 OMZ pattern.

150 Following these lines of evidence, it can be summarized that WAS upwelling initiated during the Middle to Late  
151 Miocene during the Middle Miocene Climatic Transition (MMCT), marked by cooling sea surface temperatures  
152 (SSTs) since ~14.7 Ma (Zhuang et al., 2017; Holbourn et al., 2014, 2015). Monsoonal winds subsequently  
153 intensified only after the MMCT at ~13 Ma, in conjunction with OMZ expansion to the Maldives (Betzler et al.,  
154 2016) before reaching maximum intensity at ~11 Ma and potentially declining at ~9 Ma (Bialik et al., 2020a).  
155 Upwelling re-intensified later in the Miocene and oscillated into the Plio-Pleistocene (Kroon et al., 1991; Huang  
156 et al., 2007b; Gupta et al., 2015; Tripathi et al., 2017; Alam et al., 2022). The Serravallian upwelling intensification  
157 is accompanied by significantly increased biogenic silica accumulation across the northern Indian Ocean (Keller  
158 and Barron, 1983; Baldauf et al., 1992). This biogenic silica bloom is dominated by siliceous plankton such as  
159 diatoms and radiolaria (Nigrini, 1991), indicating a sustained regime of high nutrient levels, which was able to  
160 support these primary producers (Blain et al., 1997; Schiebel et al., 2004; Mikaelyan et al., 2015).

161 With the present study, we aimThe present study aims to better constrain the relationships and interactions between  
162 different plankton groups in the WAS within the context of the dynamic changes occurring in the Oman Margin  
163 upwelling cell throughout the Middle to Late Miocene.

## 164 2. ODP Site 722 – Site location, age model, and existing dataoceanographic setting

165 Ocean Drilling Project (ODP) Site 722 (16°37'18.7" N/59°47'45.33" E) lies offshore Oman on the Owen Ridge, a  
166 300-km-long and 50-km wide feature in the WAS (Fig. 1a). Site 722 is located at a water depth of 2027.8 m  
167 (Shipboard-Scientific-Party, 1989) at the edge of the present-day Oman upwelling zone (Fig. 1a), and lies below  
168 within the core of the Indian Ocean Oxygen Minimum Zone (OMZ), with oxygen concentrations  $< 2 \mu\text{mol kg}^{-1}$   
169 persisting at a depth between c. 200 – 1000 m water depth (McCreary et al., 2013; Garcia et al., 2018).

170 The sedimentary cover at the site location comprises nannofossil, foraminifer, and diatom-rich pelagic oozes, with  
171 silty clay (Shipboard-Scientific-Party, 1989; Rodriguez et al., 2014; Bialik et al., 2020a). Bialik et al. (2020a)  
172 recently published a revised age model for Site 722, which we will utilize throughout this study. The age-depth  
173 correlation relies on biostratigraphic information obtained from the nannofossil assemblage data used in this study,  
174 combined with existing shipboard data (Shipboard-Scientific-Party, 1989). The age model covers the study interval  
175 over the Middle Miocene to the Late Miocene (c. 15.0 – 8.5 Ma, corresponding to a core depth of 276.62 to 404.94

Formatted: Superscript

176 mbsf). Bialik et al. (2020a) further published benchtop x-ray fluorescence (XRF)-based elemental data, total  
177 organic carbon content (TOC), and the calcite equivalent carbonate content in the analyzed samples. These  
178 geochemical proxy data were subsequently used in conjunction with the nannofossil assemblage data to fully  
179 constrain the response of the assemblage to ~~changing~~ environmental conditions in the WAS upwelling  
180 zone.

181 ~~The modern-day water mass configuration of the WAS (Fig. 1b) indicates that is further visualized in Figure 1.~~  
182 ~~We note that at present upwelling waters in the WAS, are generally Indian Central Waters (ICW) upwells in the~~  
183 ~~upwelling region offshore oman. The ICW which results from a mixture of warm, highly saline Red Sea and~~  
184 ~~Persian Gulf Waters (RSPGW), as well as Sub-Antarctic Mode and Intermediate Waters (SAWM, and AAIW~~  
185 ~~respectively). Present day Modern data-oceanographic research suggests that AAIW/SAMW, which contributes to~~  
186 ~~the ICW is the dominant source of nutrients in the Arabian Sea upwelling region today (Böning and Bard, 2009;~~  
187 ~~Toggweiler et al., 2019a; You and Tomczak, 1993; You, 1997, 1998). In addition, at present, there also exists~~  
188 ~~some contribution of the Indonesian Intermediate Waters (IIW), the ICW in the WAS (Fig. 1a and 1b). Therefore,~~  
189 ~~changes in the supply of these water masses are a critical aspect of understanding the region's past and likely future~~  
190 ~~upwelling dynamics (Böning and Bard, 2009; Laufkötter and Gruber, 2018; Toggweiler et al., 2019b). The Middle~~  
191 ~~to Late Miocene was similar to the modern (Bialik et al., 2019; Hall, 2012). However, the Indonesian Throughflow~~  
192 ~~region's configuration remains largely enigmatic, with potentially large emergent island chains and extensive coral~~  
193 ~~reefs between Australia and South East Asia (Hall, 2012). Deep and Intermediate water exchange and, thus, IIW~~  
194 ~~formation may thus have been restricted in the Miocene. If present, IIW likely would supply additional nutrients,~~  
195 ~~including a significant amount of bioavailable silica, to the upwelling zone in the WAS (You and Tomczak, 1993;~~  
196 ~~You, 1997). Waters in the WAS therefore represent mixture of SAMW/AAIW and IIW with ICW, which later~~  
197 ~~intermix with the regionally formed RSPGW (Böning and Bard, 2009; Toggweiler et al., 2019a).~~

### 198 3. Methods

#### 199 3.1. Nannofossil and ~~s~~Siliceous ~~f~~Fragment counts and quantification

200 We produced smear slides from 71 freeze-dried samples taken from Hole 722B (supplementary data 1) following  
201 the quantitative drop technique of Bordiga et al. (2015). On each slide, at least 47 field views were counted until  
202 at least 300 specimens were recorded or until over 190 field views were reached for samples containing very low  
203 abundances. During counting, nannofossils were identified down to the species level whenever possible. The  
204 occurrence of diatom frustules (including pennate and centric forms), as well as other biogenic silica fragments  
205 (including silicoflagellates and radiolarian fragments), were quantitatively recorded without further taxonomic  
206 identification (supplementary data 1). All recorded nannofossil taxa (+ siliceous fragments) were then converted  
207 into absolute abundances per g/sediment, according to Bordiga et al. (2015), with portions of the dataset already  
208 published (Bialik et al., 2020a). In addition to the above-described quantification, the high amount of biogenic  
209 silica recorded in some sections often dilutes absolute nannofossil abundances, ~~to alleviate the issues with potential~~  
210 ~~dilution of nannofossil abundance due to high fluxes of biogenic silica, we calculated nannofossil and siliceous~~  
211 ~~fragment fluxes for the studied interval (see section 3.5).~~

##### 212 3.1.1. Taxonomic Remarks

213 We relied on the Nannotax3 website (Nannotax 3, 2023) for detailed taxonomic reference and identification. In  
214 addition, taxonomic identification followed the concepts outlined in Perch-Nielsen (1985) and Young (1998), the

215 Handbook of Calcareous Nannoplankton 1–5 (Aubry, 1984, 1988, 1989, 1990, 1999), and the compilation on the  
216 taxonomy of the order Discoasterales by Aubry (2021).

217 For subsequent ecological interpretations, we combined the identified *Reticulofenestra* morphotypes into three  
218 size bins ranging from small (<3 µm) to medium (<3–5 µm) and large (>5 µm). There is some debate regarding  
219 the taxonomic distinction of the reticulofenestrids (genus *Reticulofenestra*) in the Neogene (see Young, 1998, for  
220 discussion). Several research groups (Auer et al., 2019; Gibbs et al., 2005; Imai et al., 2017; Jatiningrum and Sato,  
221 2017; Wade and Bown, 2006) apply different size ranges to differentiate *Reticulofenestra* taxa based on placolith  
222 size. We also note that each of these size ranges may contain a multitude of genotypes (Young, 1998). In this  
223 study, we follow the species concept of Auer et al. (2019) adapted for the Middle to Late Miocene:

- 224 • *Reticulofenestra* spp. (small) cf. *R. minuta*: reticulofenestrids < 3 µm in length without a bar spanning the  
225 central area.
- 226 • *Reticulofenestra haqii*: reticulofenestrids 3–5 µm in length with an open central area.
- 227 • *Reticulofenestra antarctica*: reticulofenestrids 3–5 µm in length with a closed central area.
- 228 • *Reticulofenestra pseudoumbilicus* (small): all reticulofenestrids 5–7 µm in length.
- 229 • *Reticulofenestra pseudoumbilicus* (sensu stricto): all reticulofenestrids >7 µm in length.

### 230 3.2. Planktonic foraminifera counts and quantification

231 For ~~foraminifer~~ ~~foraminifera~~ analysis, 28 samples were freeze-dried, weighed, and wet-sieved using mesh sizes  
232 250, 125, and 63 µm. After sieving, sample residues were oven dried at 40°C. For quantitative foraminiferal  
233 analyses, the size fractions > 250 µm and 250–125 µm were examined under a stereomicroscope (Zeiss V8). In  
234 each sample, at least 200 specimens were picked and identified. In 8 samples, less than 200 specimens were found  
235 in the available material. When necessary, samples were split into smaller aliquots (splits). The total number of  
236 foraminifera in the sediment (N/g) was calculated from the number of the counted specimen and the number of  
237 splits. Relative abundances (%) were calculated for each species (see supplementary data 2 for details).

### 238 3.3. Statistical Analyses and Ordination

239 All applied statistical and ordination methods were performed using PAST4 (v. 4.11 released 2022-09-13; Hammer  
240 et al., 2001). The applied methods include correlation matrices between nannofossil taxa and XRF-based  
241 environmental proxy data for dust flux and Mn depletion, the abundance of siliceous fragments, and calcite  
242 equivalent CaCO<sub>3</sub> content (supplementary data 3). Percentage data were then arcsine-transformed before cluster  
243 analyses and ordination methods. The arcsine transformation was applied to generate a statistically viable dataset  
244 suitable for the applied clustering and ordination methods (Sokal and Rohlf, 1995; Hammer and Harper, 2006;  
245 Auer et al., 2014, 2019; Bialik et al., 2021) and applies the universal paired group method with arithmetic mean  
246 (UPGMA) with Bray-Curtis distance. Cluster stability was further evaluated by using UPGMA clustering with  
247 Euclidian distance and Ward's method.

248 The contributing taxa of each cluster were subsequently evaluated based on similarity percentage (SIMPER)  
249 analysis (Bray-Curtis similarity). The correspondence of nannofossil variability within each sample with  
250 environmental parameters was investigated using the non-metric multidimensional scaling (nMDS), where  
251 geochemical proxy data (see sect. 2; Fig. 3) were used as environmental variables and visualized as vectors within  
252 the two-dimensional coordinate space of the nMDS. Additionally, several diversity indices (see supplementary

253 data 1), including the Shannon H'-diversity, were automatically calculated for the calcareous nannofossil  
254 assemblage (Hammer and Harper, 2006).

### 255 **3.4. Published geochemical proxy data used in this study**

256 In addition to the paleobiological data generated for this study, we further apply a suite of previously published  
257 geochemical proxy data (Bialik et al., 2020a), which we utilize as additional lines of evidence to anchor the  
258 observed assemblage variation within a multiproxy framework. In brief, we apply CaCO<sub>3</sub> and TOC combined  
259 with fluxes of siliceous fragments (see section 3.5 for details), as productivity proxies. Benchtop x-ray  
260 fluorescence-derived elemental ratios further supplement this interpretation, where we apply Mn/Al ratios to  
261 quantify Mn redirection (see Bialik et al., 2020a), based on the model of Dickens and Owen (1994). The available  
262 XRF data was also used to generate a dust flux proxy based on the elemental ratio of (K+Al)/(Fe+Ti+Zr), as  
263 defined by Kuhnt et al. (2015). This dust flux proxy allows determining the accumulation of Fe, Ti and Zr bearing  
264 heavy mineral phases, compared to elements predominantly present in clay minerals (Al + K). We interpret this  
265 proxy as a qualitative proxy for wind-derived dust flux and, thus, varying wind strength at Site 722. Dustflux and  
266 wind speed are intrinsically linked to Africa's progressive aridification due to the uplift of the Arabian Peninsula  
267 (Zhang et al., 2014; Sarr et al., 2022). The published δ<sup>15</sup>N is also discussed in the context of the new assemblage  
268 data. Tripathi et al. (2017) interpret δ<sup>15</sup>N values > 6 ‰ seen as possible an indicator indicators for significant  
269 water column denitrification in ocean basins with oxygenated bottom waters based on the approach of . Later,  
270 proxy interpretation was already applied. Bialik et al. (2020a) also used this proxy interpretation for the Middle to  
271 Late Miocene interval at Site 722, which will be followed herein herein.

Formatted: Superscript

### 272 **3.5. Calculation of accumulation rates and fluxes**

273 To quantify flux rates we applied moisture and density (MAD) derived bulk density data generated during Leg  
274 117 (Shipboard-Scientific-Party, 1989), to calculate mass accumulation rates (MAR). To calculate bulk MARs we  
275 applied linear interpolated dry bulk density for each sample point using the calculation

$$276 \quad BMAR = \frac{DBD \times LSR}{10}$$

Formatted: Centered, Space Before: 6 pt, After: 6 pt

277 Where BMAR is the bulk mass accumulation rate in g/cm<sup>2</sup>/kyr, and DBD is the dry bulk density in g/cm<sup>3</sup> based  
278 on shipboard MAD data, and LSR is the linear sedimentation rate in m/myr calculated based on the age model of  
279 Bialik et al. (2020a). Thusly generated bulk MARs were subsequently used to also calculate mass fluxes of TOC,  
280 CaCO<sub>3</sub> given as g/cm<sup>2</sup>/Ma. Fossil fluxes are given as nannofossil accumulation rates (NAR) as well as diatom  
281 accumulation rates (DAR), which are calculated by multiplying the BMAR with the number of individuals per g  
282 of sediment.

Formatted: Superscript

Formatted: Subscript

Formatted: Superscript

## 283 **4. Results**

### 284 **4.1. Calcareous Nannofossils**

#### 285 **4.1.1. Nannofossil abundance, diversity**

286 Nannofossil preservation found to be good to moderately good based on visual evaluation using light and scanning  
287 electron microscopy. Overall preservation in biogenic-silica-rich samples was noted to be slightly poorer than in  
288 samples with little or no biogenic silica.



289 Total nannofossil abundances-fluxes range from  $4.778.74 \times 10^8$  to  $5.42 \times 9.93 \times 10^{10}$  liths/per g/CaCO<sub>3</sub>cm<sup>2</sup>/Ma, with  
290 an average of  $19.4543 \times 10^{10}$  and a median of  $17.0732 \times 10^{10}$ . By comparison, total nannofossils per g/sed. range  
291 from  $2.75 \times 10^8$  to  $4.11 \times 10^{10}$  with an average of  $5.73 \times 10^9$  and a median of  $4.04 \times 10^9$ . Siliceous fragments/Diatom  
292 accumulation range from no fragments-frustules to  $1.142.41 \times 10^{10}$  per-frustules/gcm<sup>2</sup>/sedkyr, with an average of  
293  $21.240 \times 10^9$  and a median of  $31.7287 \times 10^{89}$ . In the three uppermost samples taken from Core 722B-30X, small  
294 placolith abundance (primarily *Reticulofenestra minuta*) increases sharply above the base absence (Ba) of  
295 *Reticulofenestra pseudumbilicus* (Backman et al., 2012; Agnini et al., 2017) above-after 8.8 Ma (Fig. 2). For  
296 details on the abundance and variability of individual nannofossil taxa, please refer to the supplementary material  
297 (supplementary data 1).

Formatted: Superscript

Formatted: Superscript

#### 298 4.1.2. Clusters and Ordination

299 Cluster analysis (UPGMA, Bray-Curtis similarity) resulted in 4 major clusters (clusters 1-4) that were defined at  
300 a similarity cutoff of 0.61 with a cophenetic correlation coefficient of 0.81. Clusters 1 and 4 were again split into  
301 2 (clusters 1a-b) and 3 (clusters 4a-c) sub-clusters, respectively, at a similarity cutoff of 0.66 (Fig. 4a).  
302 Bootstrapping (N=1000) shows weak support for individual clusters reflecting the overall strong similarities in the  
303 assemblage composition of the studied samples. However, one-way ANOSIM shows p-values of <0.05, indicating  
304 that the separated clusters are statistically significant.

305 Based on SIMPER analysis, the clusters and subclusters are primarily defined by the abundance variability of  
306 reticulofenestrads, discoasterids, *Cyclicargolithus floridanus*, and, to a smaller extent, *Coccolithus pelagicus*, and  
307 *Sphenolithus* spp. Based on these results, we infer that the clusters represent taphogroups, each reflecting different  
308 environmental conditions (see Auer et al., 2014).

309 Taphogroup (TG) 1a is characterized by a very high abundance of small reticulofenestrads. TG 1b is similarly  
310 characterized by a high abundance of small reticulofenestrads, although lower than TG 1a, with a higher abundance  
311 of medium reticulofenestrads and *Cyclicargolithus floridanus*. TG 2 is characterized by a high abundance of *C.*  
312 *floridanus*, and TG 3 by a high abundance of large reticulofenestrads with common discoasterids. TG 4 and its  
313 subgroups are primarily defined by the variation of the three size ranges of reticulofenestrads, with TG4a exhibiting  
314 the highest abundances of small reticulofenestrads, TG4b showing the lowest amounts of both small and medium  
315 reticulofenestrads, and through TG4c high numbers of both medium and large reticulofenestrads. See table 1 for a  
316 summary of the TGs and the supplementary material (supplementary data4) for a statistical breakdown of the  
317 contribution of all taxonomic groups to each TG.

318 The cluster analysis results are well represented within the nMDS, with TGs splitting well along coordinates 1 and  
319 2. Furthermore, the recorded stress of the nMDS is 0.13, indicating that the results are robust (Clarke, 1993). We  
320 therefore however, note the overall high compositional similarity of clusters, particularly sub-clusters, which is  
321 likely results in higher the cause of the high stress in the nMDS. However, a This is important, as recently a more  
322 conservative approach has recently been put forward, recommending that nMDS outputs exhibiting stress above  
323 0.1 should be treated with extreme cautions should be carefully evaluated (Bialik et al., 2021). We, therefore, note  
324 the overall high compositional similarity of clusters, particularly sub-clusters, which is likely the cause of the high  
325 stress in the nMDS. We found a positive loading for TOC, and siliceous fragments, along coordinates one and two.  
326 Dustflux, calculated as  $\ln((Zr+Ti+Fe)/(Al+K))$  following Kunt et al. (2015), is positively loaded on coordinate one  
327 but negatively loaded on coordinate two. The Mn/Al ratio is loaded negatively on coordinate 1 and positively on  
328 coordinate 2. Whereas CaCO<sub>3</sub> is loaded negatively on both coordinates (Fig. 4b).

329 **4.2. Planktonic Foraminifera**

330 Out of 28 samples one sample (722B-34X-3W 30-32, ca. 10.2 Ma) was barren in planktonic foraminifera. In the  
331 remaining 27 samples, 27 taxa of planktonic foraminifera were identified. The planktonic ~~foraminifer-foraminifera~~  
332 preservation was overall good, but decreases downhole. The ~~foraminifer-foraminifera~~ tests were found to be  
333 moderately pyritized. Of these taxa, 5 (*Globigerinoides ruber*, *Globorotalia menardii*, *Neogloboquadrina*  
334 *acostaensis*, *Paragloborotalia mayeri*) have their stratigraphic first or last occurrence within the studied interval.  
335 All recorded taxa were grouped according to their environmental preferences following established environmental  
336 assignments of either mixed layer taxa, open ocean thermocline taxa, open ocean sub-thermocline taxa,  
337 upwelling taxa, or unknown (Table 2).  
338 Through the studied interval, thermocline species and mixed layer taxa are the most abundant (abundance reaches  
339 more than 50%). Both mixed layer and upwelling taxa increase in prevalence through the studied interval, while  
340 thermocline species decrease. A sharp drop in thermocline taxa occurs between 11 Ma and 10 Ma, corresponding  
341 to the disappearance of *Paragloborotalia mayeri*, the dominant taxa until that time. Mixed layer taxa remain at a  
342 near-stable level from 11 Ma onwards. Upwelling taxa are not represented in two samples between 11 Ma and  
343 10.8 Ma, after which this group exhibits a steady increase until the end of the studied interval. Sub-thermocline  
344 taxa are present between 9.0 Ma and 9.5 Ma and account for only a small fraction (less than 3% at most)  
345 of the assemblage.

## 346 5. Discussion

### 347 5.1. Definition of taphogroups and their paleoenvironmental significance

348 Based on the above results, we interpret the analyzed samples in the context of their taphogroups. Taphogroups  
349 represent the total preserved fossil assemblage deposited at a given time in the past. Samples assigned to contain  
350 the same taphogroup can therefore be assumed to reflect similar local surface water conditions at Site 722.

351 **Taphogroup 1a:** TG1a is dominated by small reticulofenestrads. We, therefore, interpreted this TG as  
352 indicative of high nutrient levels facilitating the proliferation of small bloom-forming placoliths (primarily  
353 *Reticulofenestra minuta*; see Table 1). Small reticulofenestrads are commonly associated with high  
354 terrigenous nutrients in near-shore environments (see references in Table 1). However, as Site 722 was  
355 always located in the open ocean and sedimentological data (Bialik et al., 2020a) does preclude a change  
356 in terrigenous nutrient sources, a different mechanism must be invoked for this dominance of small  
357 reticulofenestrads. Studies based on coccolithophore cultures indicate that the proliferation of small  
358 placoliths may result from nitrogen limitation in a highly productive open marine environment. For  
359 example, Paasche (1998) showed that modern-day coccolithophores tend to increase the formation of small  
360 placoliths during N-limitation. Hence, we assume that the proliferation of small reticulofenestrads in the  
361 open ocean results from increasing nitrogen limitation compared to other macro- or micronutrients. Such  
362 N-limited environments often persist in settings with high productivity, due to rapid N-loss during  
363 denitrification (Paerl, 2018), which would fit with the above interpretation of small Reticulofenestrad  
364 proliferation at Site 722, offshore Oman.

365 **Taphogroup 1b:** The presence of common *C. floridanus* in combination with abundant small and medium-  
366 sized reticulofenestrads within this assemblage indicates elevated nutrient ~~sources-levels, compared to a~~  
367 fully oligotrophic assemblage (see Table 1). The very high but not dominant abundance of small  
368 reticulofenestrads may also point to N-limited nutrient sources (see TG 1a). This will be analogous to the  
369 fringes of the modern-day Arabian Sea upwelling cell, where nitrogen may be the primary limiting nutrient  
370 (Anju et al., 2020), hinting at the presence of more costally confined upwelling during TG1b, which did  
371 not fully reach Site 722—The overall high diversity, compared to other TGs, suggests that also likely  
372 oligotrophic conditions may have persisted at times (likely seasonally), which may also be-point towards  
373 phosphate co-limitationed-in at times where upwelling was limitedat-times. We thus interpret TG 1b as  
374 reflective of open marine conditions with only somewhat elevated nutrient levels compared to an open  
375 ocean gyre. Primary nutrient supply, however, is still ~~basically~~-controlled by nutrients derived through the  
376 remineralization of locally produced particulate organic matter (Cullen, 1991), likely supplied to the surface  
377 water through seasonal mixing during limited summer monsoons.

378 **Taphogroup 2:** Within TG 2, common *C. floridanus* occurs together with medium and large  
379 reticulofenestrads, commonly associated with warmer water temperature, a deep nutricline, and potentially  
380 elevated nutrient conditions. Therefore, we interpret this TG to reflect open marine conditions without  
381 directly indicating upwelling-derived nutrients. Nutrients were likely mainly derived through POM  
382 remineralization, with low external nutrient influx through upwelling or terrigenous nutrients.

383 **Taphogroup 3:** ~~We interpret TG 3 as reflecting high nutrient conditions with potentially seasonal~~  
384 stratification—Previous studies (Auer et al., 2014; Lohmann and Carlson, 1981) generally associated large  
385 reticulofenestrads with high nutrient conditions. Imai (2015) states that dominant large reticulofenestrads

386 and common discoasterids indicate low nutrient conditions and a deep nutricline compared to a high  
387 abundance of small reticulofenestrads.  
388 -However, this interpretation is questioned by the association of TG 3 with high TOC, high dust flux, and  
389 high silica accumulation rates, indicating strong upwelling conditions (Fig. 4b). ~~Similar~~ Although, similar  
390 co-occurrences of diatoms and discoasterids were previously recorded in the eastern equatorial pacific and  
391 the Mediterranean (Backman et al., 2013).  
392 ~~-In particular~~ While difficult to ascertain, the association of TG 3 with high dust flux and thus additional  
393 iron fertilization suggests that TG 3 is associated with ~~may represent~~ exceptionally high primary  
394 productivity (Guieu et al., 2019). Furthermore, modern analogs based on large *Geophyrocapsa* taxa,  
395 descendants of the genus *Reticulofenestra* (Samtleben, 1980; Perch-Nielsen, 1985; Nannotax 3, 2023), are  
396 more abundant in high nutrient upwelling zones (Bollmann, 1997).  
397 ~~This discrepancy in the interpretation of TG 3 with available environmental data could be partially~~  
398 ~~addressed by extreme seasonality~~ Seasonality, between summer monsoon and weak or absent winter  
399 monsoon however, could also serve to partially address this discrepancy in the interpretation of TG 3 with  
400 available environmental data. In such a setting, diatom and coccolithophore accumulation occurs Diatom  
401 and coccolithophore accumulation occur in such a setting in different nutrient regimes. Modern-day culture  
402 studies of coccolithophores (Paasche, 1998) also show that the calcification of coccolithophores increases  
403 during nitrogen excess and phosphate limitation.  
404 -Therefore, we interpret TG 3 as indicative of high-likely the strongest summer monsoon controlled  
405 upwelling during for our Middle to Late Miocene study interval. Conversely, a still relatively weak winter  
406 monsoon resulted in the Miocene summer monsoon season and with a deep nutricline during the rest of  
407 the year. ~~Similar co-occurrences of diatoms and discoasterids were previously recorded in the eastern~~  
408 ~~equatorial pacific and the Mediterranean~~ (Backman et al., 2013).  
409 **Taphogroup 4a:** Taphogroup 4a is not dominated by a specific reticulofenestrads size range while also  
410 containing a diverse assemblage in general (see Table 1). We, therefore, interpret this TG to show weaker  
411 upwelling conditions compared to TG3 or TG 1a during transient climatic conditions. Furthermore, weaker  
412 productivity is implied by a stronger association of TG 4a with higher Mn/Al values (Fig. 4b).  
413 **Taphogroup 4b:** The high dominance of large reticulofenestrads of TG 4b would suggest elevated,  
414 upwelling-derived nutrient levels in a temperate upwelling zone (see TG3 above). Furthermore, the size of  
415 experimental studies of calcification rates by Paasche (1998) may also be indicative of p-limitation. High  
416 nutrient conditions are corroborated by the general association of TG 4b with siliceous fragments, TOC,  
417 and dust flux in the nMDS (Fig. 4b).  
418 **Taphogroup 4c:** Taphogroup 4c is defined by both medium and large reticulofenestrads (Table 1,  
419 supplementary material). Therefore, we interpret this TG as indicative of weaker but sustained upwelling  
420 conditions. In addition, it shows some association with upwelling indicators such as dust flux and no  
421 association with the Mn/Al ratio in the sediment (Fig. 4b), indicating that it only occurs during active  
422 associated with a overall active upwelling zone and and active Mn-ridirect and therefor OMZ conditions at  
423 Site 722.  
424

## 425 5.2. Temporal Progression of Environmental Changes

426 Individual taphogroups represent specific ecospace, but to understand the relation and transitions between these  
427 ecospace, in their temporal context, their variability has to be considered in relationship to other proxies, within  
428 a multi-proxy approach. Integrating the analyses of nannofossil taphogroups (Table 1), planktonic foraminifera  
429 data (Fig. 5), the abundance of siliceous fragments, diatom fluxes and geochemical data (Bialik et al., 2020a), we  
430 delineate temporal intervals in Site 722. These reflect stratigraphic intervals of specific environmental conditions  
431 in the WAS.

432 **Interval 1 (Base of study interval – 13.4 Ma):** This interval is characterized by variable taphogroups belonging  
433 to TG 1a, TG 2, TG 4a, and TG 4b. The variable taphogroups reflect a diverse and variable nannofloral assemblage  
434 in this interval. Overall the nannofloral assemblages are characterized by an overall high abundance of  
435 *Cyclicargolithus floridanus* (Fig. 5). However, *Cyclicargolithus floridanus* abundances decline through the  
436 interval to its stratigraphic Top (T) occurrence at Site 722. In addition, we record abundant small reticulofenestrads  
437 and peaks of discoasterids (TG 4a, 4b). The average number of taxa in interval 1 is  $14.9 \pm 2.1$  ( $N = 13$ ), with an  
438 average Shannon H' diversity of  $1.6 \pm 0.4$ .

439 The planktonic foraminifera assemblage is dominated by thermocline-dwelling taxa (predominantly *P. mayeri*).  
440 Siliceous fragments are absent. We interpret this interval as a relatively low nutrient environment based on the  
441 above multi-group assemblage composition. In particular, the presence of TG 1a and 2 points to only moderately  
442 elevated nutrient concentrations in the surface waters at Site 722 during MMCT. The common occurrence of  
443 *Sphenolithus* spp. and discoasterids suggests intermittent – potentially seasonal – stratification. These results are  
444 consistent with the relatively warm SSTs recorded during this interval (Zhuang et al., 2017), further supporting a  
445 generally muted upwelling regime in the WAS during interval 1. These assumptions are corroborated by a more  
446 limited OMZ extent in the Indian Ocean, compared to the later Miocene. At Site 722 this is shown, evidenced by  
447 elevated but declining Mn content. On the Maldives, high Mn concentrations, as well as the absence of notable  
448 drift deposits, and thus lower wind intensity, also corroborates a generally weaker OMZ during this time, in the  
449 Maldives (Bialik et al., 2020b; Betzler et al., 2016).

451 **Interval 2a (13.4 – 12.0 Ma):** Interval 2a is solely comprised by TG 4c. This taphogroup is characterized by a  
452 diverse assemblage with abundant *R. pseudoumbilicus* and common medium-sized reticulofenestrads and  
453 discoasterids. The average number of taxa is  $16.6 \pm 2.2$  ( $N = 7$ ), with an average Shannon H' index of  $1.8 \pm 0.3$ .  
454 Siliceous fragments are absent.

456 Planktonic foraminiferal assemblages are dominated by thermocline species with increased abundances of mixed  
457 layer species compared to interval 1. Within interval 2a, a first slight increase in upwelling indicative taxa  
458 (primarily *G. bulloides*) is observed. We interpret this interval as indicative of a first shallowing of the thermocline  
459 due to the initial strengthening of the wind-driven upwelling regime at Site 722. This intensification is likely related  
460 to an intensification of the monsoon system following the end of the MMCT (Betzler et al., 2018). The  
461 intensification of the monsoon system is also consistent with the establishment of an increased OMZ extent and  
462 drift deposits in the Maldives (Betzler et al., 2016).

Formatted: Space After: 18 pt

463  
464 **Interval 2b (12.0 Ma – 11.0 Ma):** Interval 2b comprised primarily of assemblages belonging to TG 4c, with one  
465 sample belonging to cluster 1b. The interval similar to interval 2a is characterized by assemblages (TG4c) with  
466 abundant medium-sized reticulofenestrads that occur together with an increase in large reticulofenestrads.  
467 Furthermore, we detect a low but noteworthy increase in *Umbilicosphaera jafari* and a decline in Discoasteraceae.  
468 Furthermore, the abundance of small reticulofenestrads is lower than in interval 2a. These differences within the  
469 assemblage are also the reason why interval 2 was separated into the two sub-intervals. The average number of  
470 taxa in interval 2b is  $15.6 \pm 2.6$  ( $N = 16$ ), with an average Shannon H' index of  $1.5 \pm 0.3$ . The base of interval 2b  
471 also contains the first occurrence of diatoms within the section. Planktonic foraminifera mixed layer taxa decrease  
472 noticeably while upwelling taxa further increase in this interval.  
473

474 We interpret this interval to mark a progressive intensification in the upwelling of high-nutrient subsurface waters.  
475 We base this on 1) the increase in siliceous fragments (diatoms and other siliceous biota), 2) higher abundances of  
476 upwelling indicative planktonic foraminiferal taxa, 3) generally nutrient-adapted nannofossil taxa (i.e., medium  
477 and large sized reticulofenestrads; Beltran et al., 2014; Auer et al., 2015; Imai et al., 2015) show progressive  
478 abundance increases. Intensified upwelling is consistent with increasing  $\delta^{15}\text{N}$  values and continuous cooling at  
479 Site 722 (Zhuang et al., 2017; Bialik et al., 2020a). Increased upwelling-derived nutrient access in the northern  
480 Indian Ocean is further supported by increased productivity and nitrogen utilization in the Maldives (Betzler et al.,  
481 2016; Ling et al., 2021). The upwelling intensification after 12 Ma is consistent with an overall increase in global  
482 atmospheric circulation and oceanic current strength, [including the Indian Ocean south equatorial current](#) (Fig. 6;  
483 House et al., 1991; Gourelan et al., 2008; Groeneveld et al., 2017; Betzler and Eberli, 2019).  
484

485 **Interval 3a (11.0 Ma – 9.6 Ma):** Interval 3a is characterized by a dominance of large reticulofenestrads (*R.*  
486 *pseudoumbilicus*) (TG 3) with intermittently common discoasterids and small reticulofenestrads (TG 4b). Notably,  
487 medium-sized reticulofenestrads show very low abundances compared to the previous intervals. The abundance of  
488 *Umbilicosphaera jafari* is highly variable but overall common, while sphenoliths are rare in the lower part of the  
489 interval before increasing (up to ~40 % of the assemblage) in the upper part. Within this interval, we also note the  
490 occurrence of variable abundances of small reticulofenestrads between ~10.5 to 9.9 Ma. The average number of  
491 taxa is  $14.3 \pm 5.1$  ( $N = 22$ ), with an average Shannon H' index of  $1.1 \pm 0.4$ . The high environmental variability  
492 within this interval is illustrated by alternations between assemblages belonging to TG 3, 4b, and 4c. [Siliceous](#)  
493 [fragments](#) [Diatom fluxes](#) increase significantly ~~in abundance~~ (Fig. 5). Diatoms generally dominate the  
494 phytoplankton assemblage, even outcompeting calcareous nannoplankton in terms of total abundance. High diatom  
495 abundances are especially prevalent within samples assigned to TG 3.

496 Mixed layer taxa dominate planktonic foraminifera assemblages and increase in this interval, together with  
497 upwelling taxa. Notably, thermocline species decline to less than half of their previous abundance. One sample  
498 (722B-34X-3W 30-32) is barren of planktonic foraminifera. The lack of foraminifera is likely due to the limited  
499 sample amounts washed for this study, in conjunction with the high accumulation rates of phytoplankton (diatoms  
500 and calcareous nannofossils) in this stratigraphic interval.

Formatted: Space After: 18 pt

501 Based on the high abundance of diatoms and a generally high nutrient-adapted nannofossil assemblage, we  
502 interpret interval 3a as a peak in upwelling intensity at Site 722. This interpretation is consistent with previously  
503 published  $\delta^{15}\text{N}$  data from Site 722 and Sites U1466 and U1468, and other geochemical datasets in the Maldives  
504 (Bialik et al., 2020a; Ling et al., 2021). In addition, high productivity and OMZ expansion are further recorded by  
505 heightened TOC, Uranium accumulation, and low Mn deposition within the northwestern Indian Ocean (Dickens  
506 and Owen, 1994, 1999; Betzler et al., 2016; Bialik et al., 2020a). This corresponds to an increase in Antarctic  
507 Bottom Waters (AABW) formation due to the expansion of North Atlantic Deep Waters (NADW), indicative of  
508 an intensified global thermohaline circulation (Woodruff and Savin, 1989). Increasing numbers of discoasterids in  
509 the upper part of interval 3a, and decreasing diatoms numbers, also point towards declining upwelling and, thus,  
510 seasonal nutrient depletion when no summer monsoon-derived upwelling occurs. This pattern of clear seasonality,  
511 imparted on the plankton flux which further amplifies within the next interval.

512 **Interval 3b (9.6 Ma – 8.8 Ma):** Interval 3b continues to exhibit a dominance of large reticulofenestrads (*R.*  
513 *pseudoumbilicus*) (TG 3), although discoasterids noticeably decline and are replaced by higher abundances of  
514 sphenoliths (primarily *Sphenolithus moriformis*), with abundances of ~ 40 % of the total assemblage. Small- and  
515 medium-sized reticulofenestrads are rare in this interval. The average number of taxa is  $15 \pm 2.3$  (N = 10), with an  
516 average Shannon H' index of  $1.4 \pm 0.3$ .

517 We thus interpret interval 3b to indicate decreasing upwelling intensity based on the increase in nannofossil taxa  
518 adapted to warmer and more stratified water masses, such as *Discoaster* spp. and *Sphenolithus* spp. (Lohmann and  
519 Carlson, 1981; Castradori, 1998; Negri and Villa, 2000; Blanc-Valleron et al., 2002; Gibbs et al., 2004a; Aubry,  
520 2007; Villa et al., 2008; Schueth and Bralower, 2015). The waning upwelling of the northern Indian Ocean is  
521 corroborated by the proliferation of warm water diatom taxa in the Maldives (Site 714; Boersma and Mikkelsen,  
522 1990). Decreasing  $\delta^{15}\text{N}$  values support waning upwelling-derived productivity after 10 Ma at both Site 722 and in  
523 the Maldives and decreasing TOC fluxes at Site 722 (Gupta et al., 2015; Bialik et al., 2020a; Ling et al., 2021). It  
524 is, however, important to note that these changes are not reflected in the planktonic foraminifera community, which  
525 shows a continuously high presence of upwelling taxa (e.g., *G. bulloides*). One possibility would be that the  
526 upwelling cell became more seasonal, with nannoplankton-dominated photoautotrophic communities proliferating  
527 seasons with lower upwelling. However, primarily heterotrophic, non-symbiont-bearing taxa such as *G. bulloides*  
528 were still sustained by high primary productivity during monsoon season, as is the case in the present-day  
529 upwelling cell along the Oman Margin (Schiebel et al., 2004; Rixen et al., 2019b).

530 We assume that this waning in upwelling is related to a decrease in the hemispheric temperature gradients leading  
531 to a weaker summer monsoon wind system in the Indian Ocean. This reduction in temperature gradients is  
532 consistent with a decreasing trend in minimum deep-water temperatures, based on global benthic foraminifera  
533 compilations and deep-water records from the ninety-east-ridge (Site U1443; Fig. 1) (Lübberts et al., 2019;  
534 Westerhold et al., 2020). Furthermore, pollen data (Pound et al., 2012) suggests that progressive cooling of the  
535 northern hemisphere (NH) over the Middle to Late Miocene intensified. Northern hemisphere cooling  
536 consequently reduced the asymmetry of hemispheric temperature gradients, ~~thereby~~ thereby reducing summer monsoon  
537 wind intensity by muted northward migration of the intertropical convergence zone (ITCZ) in NH summer (Gadgil,  
538 2018; Yao et al., 2023).

539 **Interval 4 (8.8 Ma – top of study interval):** Interval 4 – consisting of only three samples – is defined by the  
540 bloom of small reticulofenestrads (*R. minuta*) in the nannofossil assemblage. We also note an elevated abundance  
541 of *Umbilicosphaera jafari* and a marked decline in *Sphenolithus* spp. relative to interval 3b. This interval consists

542 entirely of assemblages belonging to TG 1b. The average number of taxa is  $17.3 \pm 0.5$  ( $N = 3$ ), with an average  
543 Shannon  $H'$  index of  $0.5 \pm 0.0$ . Despite the high number of nannofossil taxa in this interval, the low diversity  
544 directly results from the dominance of small reticulofenestrads. Siliceous fragments (primarily diatoms) persist but  
545 are much rarer than in interval 3. This reduction in ~~siliceous fragments~~diatom fluxes is part of an ongoing decrease  
546 in biogenic silica accumulation at Site 722, which culminates in a shift from phytoplankton to zooplankton-  
547 dominated silica accumulation by  $\sim 8$  Ma (Nigrini, 1991; Prell et al., 1992). Planktonic foraminifera assemblages  
548 remains consistent with the upper part of interval 3, showing relatively high abundances of upwelling and mixed-  
549 layer taxa. We interpret this interval as a new nutrient regime ~~related which likely led~~ to a significant turnover in  
550 coccolithophore species around the same time (Young, 1990; Imai et al., 2015). However, the low sample number  
551 in this interval limits further interpretation.

### 552 5.3. Plankton community responses ~~to changing nutrient regimes~~paleoenvironmental changes

553 Based on the intervals defined by the nannofossil taphogroups, a progression of plankton communities becomes  
554 apparent within the Middle to Late Miocene at Site 722. Their variation highlights the strong interactions between  
555 monsoon wind strength, nutrient availability, and primary productivity. Therefore, we link our new assemblage  
556 data with an extensive data compilation highlighting a progressive upwelling increase, which leads to thermocline  
557 shoaling. This thermocline shoaling, in turn, results in declining sea surface temperatures, temperature decline and  
558 increased surface water productivity through the upwelling nutrient-rich thermocline waters along the Oman  
559 Margin during this time (Fig. 3; Zhuang et al., 2017; Bialik et al., 2020a).

560 Declining high Mn/Al ratios and diverse nannofossil assemblages point towards a relatively low nutrient regime  
561 between 15.0 and 13.5 Ma. Patterns of Mn decline have been observed since at least 15 Ma in the Maldives, which  
562 is in line with observations at Site 722 (Betzler et al., 2016; Bialik et al., 2020a, b). This period thus represents a  
563 progressive increase in upwelling intensity during the MMCT as a result of due to globally declining SSTs and sea  
564 levels following the end of the MCO (Zhuang et al., 2017; Miller et al., 2020). Both nannoplankton and planktonic  
565 foraminifera reflect primarily open marine, low-nutrient conditions. ~~Thermocline-dwelling taxa dominate~~  
566 ~~planktonic foraminifer assemblages, indicative of a shallow and poorly ventilated thermocline~~ (Sexton and Norris,  
567 2011; Lessa et al., 2020). ~~Nannoplankton communities further highlight a progressive change in environmental~~  
568 ~~conditions within this timeframe, as indicated by a high cluster variability after 14 Ma (Fig. 5).~~

569 By 13.5 Ma, these progressive changes culminate in a first sustained community shift in both nannofossil and  
570 planktonic foraminifera records. ~~The changes are reflected by a shift towards more nutrient-adapted taxa, such as~~  
571 ~~increasing *C. pelagicus* and decreasing sphenolith abundances. Furthermore, increased total and relative~~  
572 ~~abundances of medium and large reticulofenestrads are also observed (Figs. 2 & 5).~~

573 ~~These~~  
574 ~~abundance changes in high nutrient-adapted primary producers coincide with increases in mixed-layer dwelling~~  
575 ~~planktonic foraminifer taxa~~ We ~~We~~ consider these shifts to be a coupled response of primary producers Site 722  
576 phytoplankton communities to increased surface water nutrient levels that ~~are~~ subsequently allowed ~~by~~  
577 population increase of heterotrophs such as foraminifera. ~~Nannofossil communities also show a clear shift towards~~  
578 ~~more nutrient-adapted taxa, such as increasing *C. pelagicus* and decreasing sphenolith abundances. We interpret~~  
579 ~~this~~ ~~These changes are~~ ~~change as the~~ consistent with establishing establishment of a more pronounced upwelling  
580 regime, which also resulted in the expansion of the OMZ further into the Indian Ocean, reaching the Maldives by



581 ~13 Ma. Furthermore, available TOC data still show low accumulation rates at Site 722 at this time, indicating  
582 that organic matter was still recycled mainly within the expanding OMZ (Bialik et al., 2020a).

583 ~~This regime continued until~~By ~12 Ma, ~~when another phytoplankton -further community shift~~ shift in the  
584 nannofossil taxagroups is detected within (see interval 2b) leads to a size increase in the. ~~Medium-sized~~  
585 ~~reticulofenestrads, lower nannoplankton diversity, become dominant within the reticulofenestrads and significantly~~  
586 ~~increase their total abundance. At the same time, and a higher abundance of thermoelne-thermoelne-dwelling~~  
587 ~~planktonic foraminifer taxa~~foraminifer increase abundance and mixed-layer taxa decrease. Additionally, the  
588 ~~overall nannofossil assemblage sees a decrease in diversity, coupled with the first but still rare and intermittent~~  
589 ~~occurrences of diatoms within the record (Fig. 5). Within this interval, Together with increasing TOC accumulation~~  
590 ~~is also increasing for the first time above 0.5 wt.% TOC fluxes (Fig. 3), all these shifts point towards increasing~~  
591 ~~productivity and generally shows an increasing trend through interval 2b.~~ These changes, however, happen without  
592 any significant changes in overall temperature within the upwelling zone (Zhuang et al., 2017).

593 -A northward shift of the southern hemisphere westerlies is recorded by 12 Ma (Groeneveld et al., 2017). We  
594 hypothesize that this shift and a potential increase in wind strength may have also ~~amplified-increased the retention~~  
595 ~~of nutrient concentrations~~ in intermediate water masses within the sub-Antarctic frontal system ~~simultaneously~~.  
596 This interpretation would be in line with the effect increasing sea ice cover would have had on intermediate water  
597 ~~transportation-nutrient concentrations~~ based on modelling data and evidence from southern hemisphere records  
598 (Sarmiento et al., 2004; Sarmiento and Gruber, 2013; Laufkötter and Gruber, 2018; Groeneveld et al., 2017). Such  
599 enhanced nutrient transport within the thermocline would reconcile increased productivity without increasing the  
600 total volume of upwelling – and consequently reducing SSTs - along the Oman Margin. The first occurrence of  
601 diatoms within this interval may also point towards a shift in nutrient availability and increased phosphorus and  
602 silicon availability within the upwelling cell and likely globally (Keller and Barron, 1983). Decreasing P- and Si-  
603 limitation would thus provide more favourable conditions for highly efficient photosynthesizers, such as diatoms  
604 within the water column (Schiebel et al., 2004; Brembu et al., 2017; Sarmiento and Gruber, 2013). Within the  
605 plankton community, we also note the first intermittent occurrences of elevated *G. bulloides* abundances,  
606 indicative of high productivity upwelling conditions (Kroon et al., 1991; Gupta et al., 2015).

607 By 11 Ma, global climatic shifts and further decreasing sea levels (Miller et al., 2020; Westerhold et al., 2020) led  
608 to ~~an apparent intensification of another step in the upwelling water masses upwelling in the WAS (Fig. 6).~~ ~~As~~  
609 ~~evidenced by decreasing SSTs and further community shifts within the plankton communities.~~ ~~As a result of these~~  
610 ~~water mass changes, diatoms dominated the mineralizing our phytoplankton record primary producers~~ by 11 Ma,  
611 ~~outpacing nannoplankton for the first time, while we note~~. ~~Nannoplankton communities responded to decreasing~~  
612 ~~SSTs and increased nutrient levels with declining diversity and a high abundance of large reticulofenestrads, which~~  
613 ~~dominate the assemblage. We also note that discoasterids are particularly common within the assemblage~~  
614 ~~throughout interval 3. Within the planktonic foraminifer community, mixed-layer taxa increase. Additionally, by~~  
615 ~~11 Ma, we note~~ a first sustained occurrence (> 25 %) of *G. bulloides*. ~~Together we interpret~~ ~~these changes to~~  
616 ~~indicate~~ herefore, we interpret this shift as the inception of sustained primary productivity within the upper water  
617 column of an upwelling cell supplied with enough Si, as well as P and N to sustain a large diatom population  
618 (Brzezinski, 1985; Sarmiento and Gruber, 2013; Closset et al., 2021).

619 However, ~~these conditions are not easily reconciled with~~ the abundance of discoasterids and sphenoliths within  
620 our nannofossil record (Fig. 5) still needs to be reconciled with this interpretation. Both taxa are considered to be  
621 indicative of low nutrient conditions and increased stratification (Gibbs et al., 2004a; Schueth and Bralower, 2015;

622 Karatsolis and Henderiks, 2023). This information is thus contrary to our recorded high abundances of mixed layer  
623 dwelling foraminifera and high nutrient-adapted diatoms dominating the phytoplankton record. A possible way of  
624 integrating these opposite requirements is to evoke a highly seasonal upwelling cell with strong upwelling in one  
625 season and calm and stratified surface waters providing a deep thermo- and nutricline in the other.

626 This seasonal variability is most evident after 9.6 Ma when *Sphenolithus* abundances also increase together with  
627 overall nannofossil diversity (Fig. 5, interval 3b). These changes in the nannofossil community are also associated  
628 with decreasing diatom abundances and TOC fluxes, while upwelling indicative planktonic ~~foraminifer~~  
629 foraminifera taxa remain common. It thus seems that an initial spike in upwelling and, therefore, diatom  
630 accumulation waned again, pointing towards a significant reorganization of the upwelling cell after 9.6 Ma.

631 Within the topmost three samples of the record, belonging to interval 4, we note an increase in small  
632 reticulofenestrids corresponding to the base absence of *Reticulofenestra pseudumbilicus* around 8.8 Ma,  
633 according to accepted nannofossil biostratigraphy (Young, 1990; Backman et al., 2012; Imai et al., 2015). We note  
634 that this significant size change and an increase in small placoliths are very pronounced within our WAS records  
635 from Site 722, in agreement with Young (1990). While we cannot contribute to the discussion if this assemblage  
636 shift constitutes an evolutionary-driven adaptation of taxa within the genus *Reticulofenestra* or purely an  
637 ecophenotypically driven size adaption (Young, 1990; Imai et al., 2015). We still note that a clear link to changing  
638 nutrient levels within the upwelling cell is becoming apparent. Imai et al. (2015) further hypothesized that the size  
639 shift is related to nutrient increases within the Indo-Pacific. Based on our records of high nutrient conditions and  
640 likely at least intermittent seasonal eutrophication persisting from at least 11 Ma, we cannot completely follow  
641 their hypotheses that increasing nutrient levels within the surface ocean were the sole driver for this size shift.  
642 Therefore, we propose that changing nutrient limitation within the mixed layer may have played an important, as-  
643 of-yet unconsidered role in defining the predominant assemblage structure within the WAS upwelling system  
644 during the Middle and Late Miocene (Fig. 7).

#### 645 5.1.5.4. Contextualizing the primary ~~Wind and nutrient fluxes as primary drivers of~~ plankton 646 community shifts

647 The modern productivity patterns and oxygen depletion in the northwestern Indian Ocean differ significantly from  
648 those observed in the studied period. For example, the increase in Mn content in the Maldives in the Pliocene  
649 (Betzler et al., 2016) suggests a significant reduction in Mn redirection, which continued until today. This is indeed  
650 visible in present-day oceanographic records, where elevated Mn concentrations are only found near the margins  
651 of the Arabian Sea (ThiDieuVu and Sohrin, 2013). Meanwhile, denitrification in the Eastern Arabian Sea appears  
652 to have only become significant during the Pliocene (Tripathi et al., 2017). These changes in productivity patterns  
653 thus may indicate that the WAS was potentially more productive during the Late Miocene than today, and  
654 potentially even supported an expanded OMZ (Dickens and Owen, 1999, 1994).

655 Despite that, we note that even in the most productive parts of the Arabian Sea, conditions are rarely eutrophic  
656 (Fig. 1a). As such, ascribing permanent eutrophic or even mesotrophic conditions to any of these assemblages is  
657 unlikely to be reasonable. On the other hand, nannofossil assemblages such as TG 3 with combined diatom  
658 occurrences possibly indicate the prevalence of mesotrophic and eutrophic conditions. Diatoms are generally less  
659 adapted to low nutrient levels, requiring much higher P and N levels to form blooms compared to coccolithophores  
660 (Hutchins and Bruland, 1998; Litchman et al., 2006). If enough nutrients (including Si) are available, they tend to  
661 outcompete coccolithophores quickly and begin to dominate the mineralizing phytoplankton community (Schiebel

**Formatted:** Outline numbered + Level: 2 + Numbering  
Style: 1, 2, 3, ... + Start at: 1 + Alignment: Left + Aligned  
at: 0 cm + Indent at: 0 cm

662 et al., 2004; Brzezinski, 1985; Closset et al., 2021). Based on modern analogs, it seems likely that shifts in the  
663 nutrient ~~saturation content~~ of upwelling waters may have played an important role in controlling the observed  
664 patterns in the plankton community along the WAS during the Middle to Late Miocene. In particular after 13 Ma,  
665 where a sustained and stable SAM regime seems to have existed during the northern hemisphere summer (Betzler  
666 et al., 2016). To disentangle these patterns we therefore focus on understanding observed patterns of the two  
667 dominant phytoplankton groups present within our record, with the context of their ecological preferences and  
668 primary nutrient requirements within our study interval.

669 The co-occurrence of diatoms, discoasterids, and sphenoliths in the upper part of the studied interval (Fig. 5) thus  
670 suggests that while nutrient levels were high, upwelling was likely highly seasonal. For the WAS, high seasonality  
671 may be the result of strengthening summer monsoon winds with no changes in winter monsoon winds (Schiebel  
672 et al., 2004; Rixen et al., 2019b; Sarr et al., 2022). Increasing summer but stable or absent winter monsoon  
673 conditions are likely the result of increased cooling in the southern hemisphere (Bialik et al., 2020a; Gadgil, 2018;  
674 Sarr et al., 2022). This asymmetric cooling strengthened the summer monsoon compared to the winter monsoon  
675 system, which only intensified ~7 Ma (Gupta and Thomas, 2003; Holbourn et al., 2018; Rixen et al., 2019b).

676 The variability in wind and upwelling intensity and their interaction with nutrient availability, thus, likely also  
677 affected the community structure and size variability of primary producers on longer geological time scales. The  
678 community structure of primary producers then exerted control on first-level consumers, such as planktonic  
679 foraminifera.

680 Upwelling-derived TOC accumulation, primary productivity assemblages, and upwelling indicative foraminifera  
681 show distinctive patterns, which are, however, not in complete agreement with wind proxies and the suggested  
682 expansion of the OMZ around 13 Ma (Betzler et al., 2016). These discrepancies resulted in a long-standing debate  
683 about the validity and usefulness of upwelling proxies as monsoonal indicators (Betzler et al., 2016; Clift and  
684 Webb, 2018; Bialik et al., 2020a; Yang et al., 2020; Sarr et al., 2022). We propose that this disagreement is  
685 primarily due to inadequate treatment of nutrient limitation and nutrient supply in conjunction with wind speed  
686 when evaluating primary productivity in the WAS (Fig. 5, 7).

687 Modern-day upwelling zones in the low-to-mid-latitudes are generally well supplied in macro-nutrients, resulting  
688 in iron-limited environments or other micro- and nano-nutrient limitations (Moore et al., 2013). However,  
689 currently, the fringing areas of upwelling zones are commonly N-limited through increased denitrification in  
690 underlying OMZs (Moore et al., 2013; Bristow et al., 2017; Anju et al., 2020; Buchanan et al., 2021; Ustick et al.,  
691 2021; Buttay et al., 2022). Within the WAS upwelling zone, major nutrients ~~such as~~ N, P, and to some degree,  
692 minor nutrients such as Si are replenished through local recycling and intermixing ~~through~~ ~~with~~ deep and  
693 intermediate water masses originating from Antarctica (Fig. 7; Sarmiento et al., 2004; Meisel et al., 2011;  
694 Sarmiento and Gruber, 2013; Laufkötter and Gruber, 2018). Iron, a key micronutrient, is primarily supplied  
695 through dust and riverine influxes from surrounding continental sources (Kunkelova et al., 2022; Moore et al.,  
696 2013; Guieu et al., 2019).

697 Accepting that the wind regime had reached peak intensity by 13 Ma following a gradual increase from the end of  
698 the MCO (Betzler et al., 2016, 2018), the significant increase in diatom abundance and TOC accumulation after  
699 12 Ma is not contemporary. Therefore, the availability of nutrients and the nutrient composition also played a key  
700 role in defining the variability between coccolithophore and diatom abundances within the WAS upwelling cell.

701 Moreover, the shift in the reticulofenestrated morphotypes (Fig. 5) may also be linked to the state of nutrient

702 limitation. Paasche (1998) also has shown that modern-day coccolithophores tend to increase the formation of  
703 small placoliths during N-limitation.

704 Therefore, the shift towards higher primary productivity after 12 Ma, including first record of diatoms at Site 722,  
705 may indicate a change in nutrient composition along the WAS without necessitating a change in monsoon wind  
706 strength. Notably, during this time, the northward expansion of the southern hemisphere westerlies shifted the  
707 position of the polar and sub-Antarctic frontal system (Fig 6). In particular, the Late Miocene sea ice expansion  
708 after 11 Ma strongly affected the Antarctic frontal system and, in turn, the nutrient enrichment of intermediate  
709 waters formed in this region (Groeneveld et al., 2017; Bijl et al., 2018; Laufkötter and Gruber, 2018). Here we  
710 propose that changes in the mode of intermediate water formation significantly increased the nutrient availability  
711 in intermediate waters in the Antarctic frontal system, resulting in modern-like downwelling dynamics around  
712 Antarctica (Fig. 7). Furthermore, many modeling studies support the assumption that climatic changes affecting  
713 the Antarctic frontal system can strongly influence global productivity patterns (Sarmiento et al., 2004; Laufkötter  
714 and Gruber, 2018; Moore et al., 2018; Taucher et al., 2022). We, therefore, propose that the Middle to Late  
715 Miocene productivity changes in the WAS offer compelling evidence for this hypothesis.

#### 716 **5.2.5.5. Synthesizing Miocene nutrient transport and monsoonal upwelling**

717 Thus far, the discussion was focused on local aspects of the record in Site 722 in the WAS and northwestern Indian  
718 Ocean. However, the interconnected nature of the oceanic circulation and nutrient rejuvenation system means that  
719 critical mechanisms may be overlooked without a global perspective. For example, modeling evidence for nutrient  
720 transport and nutrient enrichment in low-latitude upwelling cells allows for the construction of a timeline of  
721 changes along the WAS and their interaction with plankton communities. Moreover, a complete oceanic  
722 perspective allows for contextualization into the broader evolution of the ocean-atmosphere system.

723 Initial plankton community structures agree with a generally low nutrient regime in a somewhat muted wind  
724 regime, based on a large amount of deep thermocline dwelling taxa in the ~~foraminifer-foraminifera~~ community,  
725 likely following the dominant phytoplankton primary productivity in the deeper photic zone (Lessa et al., 2020).  
726 In addition, the mixed layer is dominated by a diverse nannofossil assemblage ( $H'$ -diversity of around 1.5 within  
727 intervals 1 and 2). During the MMCT, wind shear strengthened by 13 Ma, resulting in a significant global shift in  
728 ocean-atmospheric circulation exemplified in the global reorganization of carbonate-platform geometries and  
729 thermocline deepening and ventilation at Site 722, as shown by the increase in mixed-layer dwelling planktonic  
730 foraminifera (Betzler et al., 2016, 2018; Betzler and Eberli, 2019; Lessa et al., 2020).

731 Modeling studies for the WAS link the initial intensification of upwelling and wind shear to a combination of  
732 increased latitudinal temperature gradients and the emergence of the Arabian Peninsula during the Middle Miocene  
733 (Zhang et al., 2014; Sarr et al., 2022; Yang et al., 2020). Notably, while OMZ expansion and Mn redirection are  
734 evident since at least ~14 Ma at Site 722 (Bialik et al., 2020a) available productivity records support at most  
735 intermittently mesotrophic and likely P- and N-limited conditions before ~12 Ma (Fig. 5). We thus propose that  
736 the upwelling cell in the WAS was wholly influenced by strong post-MMCT winds by 13 Ma. Productivity,  
737 however, was still limited by the upwelling of comparably low nutrient intermediate waters of local origin (Fig.  
738 7). -Likely originating in the marginal seas of the northwestern Indian Ocean, these water masses may have been  
739 remnants of the Tethyan Intermediate Waters (TIW). While the Tethyan Seaway had terminated between 14 and  
740 15 Ma (Bialik et al., 2019), TIW or a similar high salinity mass (Woodruff and Savin, 1989; Smart et al., 2007)  
741 was still affecting the Northern Indian Ocean until at least 12 Ma. This remnant TIW can be considered a more

742 potent form of the modern Red Sea and Persian Gulf Intermediate Waters (RSPGW; Fig 76). These warm and  
743 salty intermediate waters may have played a much more substantial role in the WAS during the early stages of the  
744 uplift of the Arabian Peninsula (Woodruff and Savin, 1989; Tomczak and Godfrey, 2003; Chowdary et al., 2005;  
745 Smart et al., 2007; Acharya and Panigrahi, 2016). The influence of remnant TIW would also align with the high  
746 abundance of thermocline-dwelling taxa until 12 Ma, which we infer to be representative of a shallow and/or a  
747 poorly ventilated thermocline (Sexton and Norris, 2011; Lessa et al., 2020).

748 It thus seems likely that late Middle Miocene WAS upwelling may have been relatively ~~nutrient-nutrient~~-poor. We  
749 speculate that these water masses may have suppressed primary productivity, muting the influence of the  
750 increasing Findlater Jets and the emerging Arabian Peninsula (e.g., Sarr et al., 2022) compared to today. Invoking  
751 significant TIW upwelling until at least 12 Ma would further reconcile the discrepancy between the occurrence of  
752 drift deposits in the Maldives, and thus strong monsoon winds and the first clear evidence for strong upwelling in  
753 the WAS, with the abundance increase of upwelling indicative planktonic foraminifera (e.g., *G. bulloides*; Fig 5)  
754 and the first occurrence of diatoms at Site 722 (Fig 5; Kroon et al., 1991; Huang et al., 2007b; Gupta et al., 2015;  
755 Bialik et al., 2020a). This change in nutrient availability is also reflected by a contemporary increase in medium-  
756 sized reticulofenestrads (*R. antarctica* and *R. haqii*), which are generally assumed to reflect higher nutrient  
757 availability due to upwelling (Fig. 5; Auer et al., 2019 and references therein).

758 Productivity in the WAS thereby only began to increase as remnant TIW got progressively supplanted by other,  
759 more nutrient-rich, water masses. At present, the waters upwelling in the Arabian Sea is primarily regarded to be  
760 ~~ICW, which therefore also includes IIW, and nutrient-rich sub-Antarctic mode waters (SAMW)~~ and AAIW  
761 ~~Antarctic Intermediate Waters~~ (You, 1997, 1998; Böning and Bard, 2009; Munz et al., 2017; Chinni and Singh,  
762 2022). Today AAIW and SAMW forming in the northern branch of the Antarctic Divergence, control up to 75%  
763 of low-latitude productivity (Sarmiento et al., 2004).

764 We hypothesize that the increasing formation of AAIW and SAMW following the northward shift of the westerlies  
765 around 12 Ma (Fig.6) may have modulated low latitude productivity (Groeneveld et al., 2017; Laufkötter and  
766 Gruber, 2018; Moore et al., 2018; Taucher et al., 2022). This time also aligns well with the proposed inception of  
767 the northward shift of southern hemisphere climate belts and the invigoration of the south equatorial current  
768 (LeHouedec et al., 2012; Reuter et al., 2019). Following that, it can also be assumed that by 12 Ma, the northward  
769 expansion of the southern hemisphere Westerlies resulted in a near-modern Antarctic Divergence (Groeneveld et  
770 al., 2017; Laufkötter and Gruber, 2018).

771 This global change in circulation patterns was fully established by 11 Ma, with cool nutrient-rich SAMW/AAIW  
772 waters reaching Site 722, evidenced by a further SST drop (Zhuang et al., 2017). This resulted in the highest  
773 productivity in the WAS upwelling cell during the Miocene (Figs. 5–7). The Late Miocene high-productivity  
774 interval in the WAS, is thus the result of intense summer monsoon-dominated AAIW/SAMW upwelling, fueled  
775 by the Findlater Jets and forced by steep latitudinal temperature gradients and favourable tectonic conditions on  
776 the Arabian Peninsula (Pound et al., 2012; Zhang et al., 2014; Sarr et al., 2022). Summer months were thus  
777 characterized by eutrophic P-, N-, and potentially Si-enriched waters, allowing the proliferation of diatoms and  
778 other siliceous organisms. ~~In contrast, the W~~winter months, ~~in contrast,~~ favoured the accumulation of deep-  
779 dwelling discoasterids that utilized the nutrient-rich waters below a relatively deeper winter thermocline. Higher  
780 abundances of mixed-layer dwelling taxa also reflect the increased mixed-layer depth (Fig. 57). Expanding  
781 AAIW/SAMW-fueled high productivity that consequently also resulted in the highest recorded TOC fluxes  
782 between 11 – 10 Ma and a substantial OMZ expansion deep into the equatorial Indian Ocean (Dickens and Owen,

Formatted: Font: Font color: Auto

1994; Bialik et al., 2020a). Increasing OMZs also resulted in a global increase in denitrification, which is well-recorded in foraminifer-bound  $\delta^{15}\text{N}$  records, showing a trend from more oxygenated intermediate waters during the MCO to lower oxygenated waters in the Late Miocene in the Indo-Pacific (Auderset et al., 2022).

By 10 Ma, OMZs had reached a critical threshold, leading to another substantial change in nutrient conditions within the WAS upwelling. Through increased denitrification in the OMZ underlying the upwelling cell, nitrate and ammonia were lost through bacterial conversion to  $\text{N}_2$  (Sigman and Fripiat, 2019). Strong denitrification subsequently led to increasingly N-limited water masses upwelling within the WAS. Although concrete evidence is only presented for the WAS, these patterns could also have occurred globally, considering the clear evidence for decreasing ocean oxygenation during the Late Miocene (Auderset et al., 2022). The Late Miocene N-limitation in the WAS upwelling cell is chiefly expressed by a decline in diatom abundances after 10 Ma, in conjunction with overall community shifts in the nannofossil assemblage.

Total upwelling intensity also remained consistently high, as indicated by the available SST record of Zhuang et al. (2017). Primary productivity thus remained relatively high, which is characterized by the continued presence and even dominance of large reticulofenestrads, diatoms, and the continuously high TOC concentration within the sediment (often > 1 wt.%; Fig. 3). We thus assume that the drop in diatom abundance and intermittent decline in  $\delta^{15}\text{N}$  values at Site 722 (Figs. 3, 5.) were not caused by decreasing upwelling intensity but rather a decline in P and Si availability and, thus declining export of diatom-derived organic matter. The increase in sphenoliths within our Site 722 record (Fig. 5) could indicate increased environmental stress within the nannofossil assemblage (Wade and Bown, 2006). Sphenoliths are ~~here~~ likely not ~~representative—a good indicator of long-term of higher~~ stratification ~~changes~~ (Karatsolis and Henderiks, 2023) in highly seasonal upwelling regimes like the WAS, as high TOC and thus sustained, but lower, diatom fluxes indicate continued upwelling after 10 Ma at Site 722. Sustained seasonal upwelling and high organic matter export (Fig. 3) are further inferred by decreasing organic carbon  $\delta^{13}\text{C}$  throughout this interval (Bialik et al., 2020a and references therein).

By 8.8 Ma, the adaption of smaller reticulofenestrads may result~~ed to~~ in an ~~evolutionary~~ adaption to the continued N-limited nutrient availability in the WAS. We base this interpretation on the nutrient adaption of coccolithophorids based on modern culture experiments (Paasche, 1998). Although somewhat anecdotal, these offer the currently best explanation to reconcile the recorded history of Site 722 upwelling changes with the stark shifts in reticulofenestrads size ranges. It should be noted that these shifts have been recorded throughout the mid- and low latitudes of the Indopacific (Young, 1990; Imai et al., 2015). However, the full impact of this hypothesis needs to be tested further.

The data compilation of Young (1990) further shows that the recorded Late Miocene size shift was primarily limited to the low and mid-latitudes, with larger reticulofenestrads persisting within in the higher latitudes. We propose that the transition in *Reticulofenestra* morphology from large to small morphotypes thus primarily represents a significant shift in nutrient limitation rather than total nutrient availability within the mid to low latitudes. We further argue that this turnover reflects N-limitation within the low- and mid-latitudes due to sustained and intense denitrification after 12 Ma (Auderset et al., 2022). Further studies, particularly on ultrastructural morphotaxonomy of reticulofenestrads, will be needed to fully disentangle the implications of the proposed N-limited nanno-floral turnover.

The highly opportunistic small *Reticulofenestra* morphotype was subsequently also able to sustain phytoplankton blooms in the WAS, as evidenced by the significant increase in nannofossils within the sediment (Fig. 5). Furthermore, the high mass of small coccolith cells potentially also contributed to the re-establishment of strong

824 denitrification as evidenced by a rise in  $\delta^{15}\text{N}$ -values after 8.8 Ma (Fig. 3), as their additional biomass contributed  
825 to OMZ re-expansion. Detailed records of Late Miocene OMZ strength throughout the Indian Ocean will,  
826 however, be necessary to fully quantify the impact on local upwelling. Local tectonics also began to modify the  
827 region configuration at this time (Rodriguez et al., 2014), leading to bottom current intensification (Rodriguez et  
828 al., 2016), which may have also modulated subsequent OMZ dynamics (Dickens and Owen, 1999).

## 829 6. Conclusions

830 We present fully quantitative nannofossil and planktonic ~~foraminifer~~ ~~foraminifera~~ assemblage data in conjunction  
831 with diatom frustule abundances for Site 722. Within a multi-proxy framework, these novel data allowed us to  
832 disentangle the complex and long-debated changes within the upwelling system of the WAS in the Middle to Late  
833 Miocene. We show that the Findlater Jets, and thus Indian summer monsoon wind strength, are the primary drivers  
834 of upwelling. However, wind-driven upwelling is also clearly modulated by local and global water mass changes  
835 and changing nutrient fluxes. In particular, changing nutrient transport through intermediate waters has had a  
836 significant – until now unconsidered – impact on primary productivity patterns and plankton communities over  
837 the Middle and Late Miocene in the Indian Ocean. We, therefore, reach the following key conclusion:

838 (1) the expansion and evolution of upwelling within the WAS as a complex interplay of regional tectonics, global  
839 climate, and ice volume changes affected upwelling intensity and nutrient availability. The present study  
840 emphasizes that wind and nutrient changes are intrinsically related but do not necessarily operate in tandem on  
841 longer supra-Milankovitch time scales. It is, therefore, crucial to consider both water masses changes ~~as well as~~ ~~and~~  
842 atmospheric conditions when investigating past wind-driven upwelling regimes.

843 (2) The interaction first invigorated monsoonal circulation after the MMCT before resulting in the reorganization  
844 of intermediate water circulation, controlled by the inception of a near-modern configuration of the Antarctic  
845 Divergence, [which supplied nutrient rich intermediate waters to the low latitudes](#).

846 (3) These processes led to the progressive establishment of near-modern nutrient transport within the Indian Ocean  
847 by 12 to 11 Ma. Furthermore, these changes acted together with denitrification in expanding global OMZs  
848 (Auderset et al., 2022) to increase N-limitation and subsequent adaption of coccolithophorids to the new nutrient  
849 conditions in the mid to low latitudes.

850 (4) We provide a timeline of events that agrees with global climatic and local productivity patterns, which are all  
851 linked through the invigoration of upwelling cells and nutrient fluxes through intermediate water masses into the  
852 lower latitudes. In particular past changes in intermediate water mass circulation, replenishment, and expansion  
853 appear to be a key – and critically understudied – aspect within paleoceanography and paleoclimatology that is  
854 crucial to understanding past and, thereby, future low latitude productivity.

## 855 7. Data and code availability

856 Data and code are available from the supplementary material and on Pangaea (DOI: will be provided once  
857 available)

858 **8. Author contribution**

859 **GA:** designed the study, [acquired funding](#), conducted nannofossil counts and statistics, wrote the first draft, edited  
860 the text, and drafted the figures. **OMB:** designed the study, performed statistical analyses, wrote the first draft,  
861 edited the text, and helped draft the figures. **MEA:** performed planktonic ~~foraminifer~~-[foraminifera](#) taxonomic  
862 analysis and assemblage interpretation and contributed to the first draft of the text. **NVV:** helped draft the figures  
863 and contributed to data interpretation, edited the final draft of the MS. **WEP:** ~~e~~[onducted-supervised and conducted](#)  
864 foraminiferal analysis; and contributed to writing and editing of the text.

865 **9. Competing interests**

866 The authors declare that they have no conflict of interest.

867 **10. Acknowledgments**

868 [This research used samples and data provided by the](#) Ocean Drilling Program (ODP) and the [International Ocean](#)  
869 [Discovery Program \(IODP\)](#). ~~The authors acknowledge funding from~~[This study was funded by](#) the Austrian  
870 Science Fund (FWF Project P36046-N; [MIO:TRANS – Nutrient Fluxes in the Miocene Indian Ocean](#)). [OMB is](#)  
871 [partially supported by the German \(GEOMAR\)-Israeli \(University of Haifa\) Helmholtz International Laboratory](#)  
872 [-The Eastern Mediterranean Sea Centre- An Early-Warning Model-System for our Future Oceans: EMS Future](#)  
873 [Ocean Research \(EMS FORE\)](#). Furthermore, the authors would like to thank all Bialik et al. (2020) authors for  
874 their invaluable contribution to this research and their expertise in interpreting the data. In particular, we would  
875 like to thank Dick Kroon for his early support of these studies and his invaluable discussions on the subject matter.



876 References

877

878 Acharya, S. S. and Panigrahi, M. K.: Eastward shift and maintenance of Arabian Sea oxygen  
879 minimum zone: Understanding the paradox, *Deep Sea Res. Part I Oceanogr. Res. Pap.*, 115,  
880 240–252, <https://doi.org/10.1016/j.dsr.2016.07.004>, 2016.

881 Agnini, C., Monechi, S., and Raffi, I.: Calcareous nannofossil biostratigraphy: historical  
882 background and application in Cenozoic chronostratigraphy, *Lethaia*, 50, 447–463,  
883 <https://doi.org/10.1111/let.12218>, 2017.

884 Alam, M., Tripti, M., Gurumurthy, G. P., Sohrin, Y., Tsujisaka, M., Singh, A. D., Takano, S.,  
885 and Verma, K.: Palaeoredox reconstruction in the eastern Arabian Sea since the late Miocene:  
886 Insights from trace elements and stable isotopes of molybdenum ( $\delta^{98}/95\text{Mo}$ ) and tungsten  
887 ( $\delta^{186}/184\text{W}$ ) at IODP Site U1457 of Laxmi Basin, *Palaeogeogr Palaeoclim Palaeoecol*, 587,  
888 110790, <https://doi.org/10.1016/j.palaeo.2021.110790>, 2022.

889 Anju, M., Sreesh, M. G., Valsala, V., Smitha, B. R., Hamza, F., Bharathi, G., and Naidu, C.  
890 V.: Understanding the Role of Nutrient Limitation on Plankton Biomass Over Arabian Sea  
891 Via 1-D Coupled Biogeochemical Model and Bio-Argo Observations, *J Geophys Res Oceans*,  
892 125, <https://doi.org/10.1029/2019jc015502>, 2020.

893 Aubry, M.-P.: *Handbook of Cenozoic Calcareous Nannoplankton: Book 1. Ortholithae*  
894 *(Discoasters)*, Micropaleontology Press, 1984.

895 Aubry, M.-P.: *Handbook of Cenozoic Calcareous Nannoplankton: Book 2. Ortholithae*  
896 *(Holococcoliths, Ceratoliths, Ortholiths and Others)*, Micropaleontology Press, 1988.

897 Aubry, M.-P.: *Handbook of Cenozoic Calcareous Nannoplankton: Book 3. Ortholithae*  
898 *(Pentaliths, and Others), Heliolithae (Fasciculiths, Sphenoliths and Others)*,  
899 Micropaleontology Press, 1989.

900 Aubry, M.-P.: *Handbook of Cenozoic Calcareous Nannoplankton: Book 4. Heliolithae*  
901 *(Helicoliths, Cribriliths, Lopadoliths and Others)*, Micropaleontology Press, 1990.

902 Aubry, M.-P.: *Handbook of Cenozoic Calcareous Nannoplankton. Book 5: Heliolithae*  
903 *(Zygoliths and Rhabdoliths)*, Micropaleontology Press, 1999.

904 Aubry, M.-P.: A major Pliocene coccolithophore turnover: Change in morphological strategy  
905 in the photic zone, vol. 424, *Geological Society of America*, 25–51,  
906 [https://doi.org/10.1130/2007.2424\(02\)](https://doi.org/10.1130/2007.2424(02)), 2007.

907 Aubry, M.-P.: *Coccolithophores: Cenozoic Discoasterales—Biology, Taxonomy,*  
908 *Stratigraphy*, 460 pp., 2021.

909 Auderset, A., Moretti, S., Taphorn, B., Ebner, P.-R., Kast, E., Wang, X. T., Schiebel, R.,  
910 Sigman, D. M., Haug, G. H., and Martínez-García, A.: Enhanced ocean oxygenation during  
911 Cenozoic warm periods, *Nature*, 609, 77–82, <https://doi.org/10.1038/s41586-022-05017-0>,  
912 2022.

913 Auer, G., Piller, W. E., and Harzhauser, M.: High-resolution calcareous nannoplankton  
914 palaeoecology as a proxy for small-scale environmental changes in the Early Miocene, *Mar.*  
915 *Micropaleontol.*, 111, 53–65, <https://doi.org/10.1016/j.marmicro.2014.06.005>, 2014.

916 Auer, G., Piller, W. E., and Harzhauser, M.: Two distinct decadal and centennial cyclicities  
917 forced marine upwelling intensity and precipitation during the late Early Miocene in central  
918 Europe, *Clim. Past.*, 11, 283–303, <https://doi.org/10.5194/cp-11-283-2015>, 2015.

919 Auer, G., DeVleeschouwer, D., Smith, R. A., Bogus, K., Groeneveld, J., Grunert, P.,  
920 Castañeda, I. S., Petrick, B., Christensen, B., Fulthorpe, C., Gallagher, S. J., and Henderiks,  
921 J.: Timing and Pacing of Indonesian Throughflow Restriction and Its Connection to Late  
922 Pliocene Climate Shifts, *Paleoceanogr. Paleoclimatol.*, 34, 635–657,  
923 <https://doi.org/10.1029/2018pa003512>, 2019.

924 Avinash, K., Manjunath, B. R., and Kurian, P. J.: Glacial-interglacial productivity contrasts  
925 along the eastern Arabian Sea: Dominance of convective mixing over upwelling, *Geosci*  
926 *Front*, 6, 913–925, <https://doi.org/10.1016/j.gsf.2015.03.003>, 2015.

927 Aze, T., Ezard, T. H. G., Purvis, A., Coxall, H. K., Stewart, D. R. M., Wade, B. S., and  
928 Pearson, P. N.: A phylogeny of Cenozoic macroperforate planktonic foraminifera from fossil  
929 data, *Biol Rev*, 86, 900–927, <https://doi.org/10.1111/j.1469-185x.2011.00178.x>, 2011.

930 Backman, J., Raffi, I., Rio, D., Fornaciari, E., and Pälike, H.: Biozonation and biochronology  
931 of Miocene through Pleistocene calcareous nannofossils from low and middle latitudes,  
932 *Newsl. Stratigr.*, 45, 221–244, <https://doi.org/10.1127/0078-0421/2012/0022>, 2012.

933 Backman, J., Raffi, I., Ciommelli, M., and Baldauf, J.: Species-specific responses of late  
934 Miocene Discoaster spp. to enhanced biosilica productivity conditions in the equatorial  
935 Pacific and the Mediterranean, *Geo-mar Lett*, 33, 285–298, <https://doi.org/10.1007/s00367-013-0328-0>, 2013.

937 Baldauf, J. G., Barron, J. A., Ehrmann, W. U., Hempel, P., and Murray, D.: Synthesis of  
938 Results from Scientific Drilling in the Indian Ocean, *Geophys Monogr Ser*, 70, 335–349,  
939 <https://doi.org/10.1029/gm070p0335>, 1992.

940 Balun, A., Field, D. B., Redondo-Rodriguez, A., and Weeks, S. J.: Greenhouse gas,  
941 upwelling-favorable winds, and the future of coastal ocean upwelling ecosystems, *Global*  
942 *Change Biol*, 16, 1213–1228, <https://doi.org/10.1111/j.1365-2486.2009.02094.x>, 2010.

943 Basavani, P.: Findlater Jet Climatology in Summer Monsoon Its Role on Onset Progress and  
944 Relation with Air Sea Interaction Parameters Over Arabian Sea, 2013.

945 Beltran, C., Rousselle, G., Backman, J., Wade, B. S., and Sicre, M.-A.: Paleoenvironmental  
946 conditions for the development of calcareous nannofossil acme during the late Miocene in the  
947 eastern equatorial Pacific, *Paleoceanography*, 29, 210–222,  
948 <https://doi.org/10.1002/2013pa002506>, 2014.

949 Berggren, W. A., Kennett, J. P., and Srinivasan, M. S.: Neogene Planktonic Foraminifera: A  
950 Phylogenetic Atlas, *Micropaleontology*, 31, 94, <https://doi.org/10.2307/1485586>, 1985.

- 951 Betzler, C. and Eberli, G. P.: Miocene start of modern carbonate platforms, *Geology*, 47, 771–  
952 775, <https://doi.org/10.1130/g45994.1>, 2019.
- 953 Betzler, C., Eberli, G. P., Kroon, D., Wright, J. D., Swart, P. K., Nath, B. N., Alvarez-  
954 Zarkian, C. A., Alonso-García, M., Bialik, O. M., Blättler, C. L., Guo, J. A., Haffen, S.,  
955 Horozal, S., Inoue, M., Jovane, L., Lanci, L., Laya, J. C., Mee, A. L. H., Lüdmann, T.,  
956 Nakakuni, M., Niino, K., Petruny, L. M., Pratiwi, S. D., Reijmer, J. J. G., Reolid, J., Slagle,  
957 A. L., Sloss, C. R., Su, X., Yao, Z., and Young, J. R.: The abrupt onset of the modern South  
958 Asian Monsoon winds., *Sci. Rep.*, 6, 29838, <https://doi.org/10.1038/srep29838>, 2016.
- 959 Betzler, C., Eberli, G. P., Lüdmann, T., Reolid, J., Kroon, D., Reijmer, J. J. G., Swart, P. K.,  
960 Wright, J., Young, J. R., Alvarez-Zarkian, C., Alonso-García, M., Bialik, O. M., Blättler, C.  
961 L., Guo, J. A., Haffen, S., Horozal, S., Inoue, M., Jovane, L., Lanci, L., Laya, J. C., Mee, A.  
962 L. H., Nakakuni, M., Nath, B. N., Niino, K., Petruny, L. M., Pratiwi, S. D., Slagle, A. L.,  
963 Sloss, C. R., Su, X., and Yao, Z.: Refinement of Miocene sea level and monsoon events from  
964 the sedimentary archive of the Maldives (Indian Ocean), *Prog Earth Planet Sci*, 5, 5,  
965 <https://doi.org/10.1186/s40645-018-0165-x>, 2018.
- 966 Bialik, O. M., Frank, M., Betzler, C., Zammit, R., and Waldmann, N. D.: Two-step closure of  
967 the Miocene Indian Ocean Gateway to the Mediterranean, *Sci. Rep.*, 9, 8842–8852,  
968 <https://doi.org/10.1038/s41598-019-45308-7>, 2019.
- 969 Bialik, O. M., Auer, G., Ogawa, N. O., Kroon, D., Waldmann, N. D., and Ohkouchi, N.:  
970 Monsoons, Upwelling, and the Deoxygenation of the Northwestern Indian Ocean in Response  
971 to Middle to Late Miocene Global Climatic Shifts, *Paleoceanogr. Paleoclimatol.*, 35,  
972 <https://doi.org/10.1029/2019pa003762>, 2020a.
- 973 Bialik, O. M., Reolid, J., Betzler, C., Eberli, G. P., and Waldmann, N. D.: Source shifts to  
974 periplatform deposits during the early to middle Miocene in response to climatic and  
975 oceanographic forcing, Maldives, western Indian Ocean, *Palaeogeogr Palaeoclim Palaeoecol*,  
976 559, 109969, <https://doi.org/10.1016/j.palaeo.2020.109969>, 2020b.
- 977 Bialik, O. M., Jarochovska, E., and Grossowicz, M.: Ordination analysis in sedimentology,  
978 geochemistry and palaeoenvironment—Background, current trends and recommendations,  
979 *Depositional Rec*, 7, 541–563, <https://doi.org/10.1002/dep2.161>, 2021.
- 980 Bijl, P. K., Houben, A. J. P., Hartman, J. D., Pross, J., Salabarnada, A., Escutia, C., and  
981 Sangiorgi, F.: Paleooceanography and ice sheet variability offshore Wilkes Land, Antarctica –  
982 Part 2: Insights from Oligocene–Miocene dinoflagellate cyst assemblages, *Clim. Past.*, 14,  
983 1015–1033, <https://doi.org/10.5194/cp-14-1015-2018>, 2018.
- 984 Blain, S., Leynaert, A., Tréguer, P., Chretiennot-Dinet, M.-J., and Rodier, M.: Biomass,  
985 growth rates and limitation of Equatorial Pacific diatoms, *Deep Sea Res Part Oceanogr Res*  
986 *Pap*, 44, 1255–1275, [https://doi.org/10.1016/s0967-0637\(97\)00014-9](https://doi.org/10.1016/s0967-0637(97)00014-9), 1997.
- 987 Blanc-Valleron, M. M., Pierre, C., Caulet, J. P., Caruso, A., Rouchy, J. M., Cespuglio, G.,  
988 Sprovieri, R., Pestrea, S., and Stefano, E. D.: Sedimentary, stable isotope and  
989 micropaleontological records of paleooceanographic change in the Messinian Tripoli  
990 Formation (Sicily, Italy), *Palaeogeogr. Palaeoclimatol. Palaeoecol.*, 185, 255–286,  
991 [https://doi.org/10.1016/s0031-0182\(02\)00302-4](https://doi.org/10.1016/s0031-0182(02)00302-4), 2002.

- 992 Boersma, A. and Mikkelsen, N.: Miocene-Age Primary Productivity Episodes and Oxygen  
 993 Minima in the Central Equatorial Indian Ocean, in: Proceedings of the Ocean Drilling  
 994 Program, Scientific Results, Vol. 115, vol. 115, edited by: Duncan, R. A., Backman, and  
 995 Peterson, L. C., <https://doi.org/10.2973/odp.proc.sr.115.162.1991>, 1990.
- 996 Bollmann, J.: Morphology and biogeography of *Gephyrocapsa* coccoliths in Holocene  
 997 sediments, *Mar. Micropaleontol.*, 29, 319–350, [https://doi.org/10.1016/s0377-8398\(96\)00028-](https://doi.org/10.1016/s0377-8398(96)00028-x)  
 998 [x](https://doi.org/10.1016/s0377-8398(96)00028-x), 1997.
- 999 Böning, P. and Bard, E.: Millennial/centennial-scale thermocline ventilation changes in the  
 1000 Indian Ocean as reflected by aragonite preservation and geochemical variations in Arabian  
 1001 Sea sediments, *Geochim. Cosmochim. Acta*, 73, 6771–6788,  
 1002 <https://doi.org/10.1016/j.gca.2009.08.028>, 2009.
- 1003 Bordiga, M., Bartol, M., and Henderiks, J.: Absolute nannofossil abundance estimates:  
 1004 Quantifying the pros and cons of different techniques, *Rev. de Micropaleontol.*, 58, 155–165,  
 1005 <https://doi.org/10.1016/j.revmic.2015.05.002>, 2015.
- 1006 Brembu, T., Mühlroth, A., Alipanah, L., and Bones, A. M.: The effects of phosphorus  
 1007 limitation on carbon metabolism in diatoms, *Philosophical Transactions Royal Soc B*  
 1008 *Biological Sci*, 372, 20160406, <https://doi.org/10.1098/rstb.2016.0406>, 2017.
- 1009 Bristow, L. A., Mohr, W., Ahmerkamp, S., and Kuypers, M. M. M.: Nutrients that limit  
 1010 growth in the ocean, *Curr Biol*, 27, R474–R478, <https://doi.org/10.1016/j.cub.2017.03.030>,  
 1011 2017.
- 1012 Brummer, G.-J. A. and Kučera, M.: Taxonomic review of living planktonic foraminifera, *J*  
 1013 *Micropalaeontol*, 41, 29–74, <https://doi.org/10.5194/jm-41-29-2022>, 2022.
- 1014 Brzezinski, M. A.: The Si: C: N ratio of marine diatoms: interspecific variability and the  
 1015 effect of some environmental variables 1, *J. Phycol.*, 21, 347–357,  
 1016 <https://doi.org/10.1111/j.0022-3646.1985.00347.x>, 1985.
- 1017 Buchanan, P. J., Aumont, O., Bopp, L., Mahaffey, C., and Tagliabue, A.: Impact of  
 1018 intensifying nitrogen limitation on ocean net primary production is fingerprinted by nitrogen  
 1019 isotopes, *Nat. Commun.*, 12, 6214, <https://doi.org/10.1038/s41467-021-26552-w>, 2021.
- 1020 Buttay, L., Vasseur, D. A., González-Quirós, R., and Nogueira, E.: Nutrient limitation can  
 1021 explain a rapid transition to synchrony in an upwelling-driven diatom community, *Limnol*  
 1022 *Oceanogr*, 67, S298–S311, <https://doi.org/10.1002/lno.12033>, 2022.
- 1023 Cao, W., Zahirovic, S., Flament, N., Williams, S., Golonka, J., and Müller, R. D.: Improving  
 1024 global paleogeography since the late Paleozoic using paleobiology, *Biogeosciences*, 14,  
 1025 5425–5439, <https://doi.org/10.5194/bg-14-5425-2017>, 2017.
- 1026 Carlson, R. E.: A trophic state index for lakes, *Limnol Oceanogr*, 22, 361–369,  
 1027 <https://doi.org/10.4319/lo.1977.22.2.0361>, 1977.
- 1028 Castradori, D.: Calcareous nannofossils in the basal Zanclean of the Eastern Mediterranean  
 1029 Sea: remarks on paleoceanography and sapropel formation, in: Proceedings of the Ocean

- 1030 Drilling Program, 160 Scientific Results, vol. 160,  
1031 <https://doi.org/10.2973/odp.proc.sr.160.005.1998>, 1998.
- 1032 Chaisson, W. P. and Ravelo, A. C.: Changes in upper water-column structure at Site 925, late  
1033 Miocene–Pleistocene: planktonic foraminifer assemblage and isotopic evidence, in:  
1034 Proceedings of the Ocean Drilling Program, 154 Scientific Results,  
1035 <https://doi.org/10.2973/odp.proc.sr.154.105.1997>, 1997.
- 1036 Chinni, V. and Singh, S. K.: Dissolved iron cycling in the Arabian Sea and sub-tropical gyre  
1037 region of the Indian Ocean, *Geochim Cosmochim Acta*, 317, 325–348,  
1038 <https://doi.org/10.1016/j.gca.2021.10.026>, 2022.
- 1039 Chowdary, J. S., Gnanaseelan, C., Thompson, B., and Salvekar, P. S.: Water mass properties  
1040 and transports in the Arabian Sea from Argo observations, *J. Atmos. Sci.*, 10, 235–260,  
1041 <https://doi.org/10.1080/17417530600752825>, 2005.
- 1042 Clarke, K. R.: Non-parametric multivariate analyses of changes in community structure,  
1043 *Australian Journal of Ecology*, 18, 117–143, <https://doi.org/10.1111/j.1442-9993.1993.tb00438.x>, 1993.
- 1045 Clift, P. D. and Webb, A. A. G.: A history of the Asian monsoon and its interactions with  
1046 solid Earth tectonics in Cenozoic South Asia, Geological Society, London, Special  
1047 Publications, SP483.1, <https://doi.org/10.1144/sp483.1>, 2018.
- 1048 Closset, I., McNair, H. M., Brzezinski, M. A., Krause, J. W., Thamtrakoln, K., and Jones, J.  
1049 L.: Diatom response to alterations in upwelling and nutrient dynamics associated with climate  
1050 forcing in the California Current System, *Limnol Oceanogr*, 66, 1578–1593,  
1051 <https://doi.org/10.1002/lno.11705>, 2021.
- 1052 Cullen, J. J.: Hypotheses to explain high-nutrient conditions in the open sea, *Limnol*  
1053 *Oceanogr*, 36, 1578–1599, <https://doi.org/10.4319/lo.1991.36.8.1578>, 1991.
- 1054 Dickens, G. R. and Owen, R. M.: Late Miocene–Early Pliocene manganese redirection in the  
1055 central Indian Ocean: Expansion of the Intermediate Water oxygen minimum zone,  
1056 *Paleoceanography*, 9, 169–181, <https://doi.org/10.1029/93pa02699>, 1994.
- 1057 Dickens, G. R. and Owen, R. M.: The Latest Miocene–Early Pliocene biogenic bloom: a  
1058 revised Indian Ocean perspective, *Mar Geol*, 161, 75–91, [https://doi.org/10.1016/s0025-3227\(99\)00057-2](https://doi.org/10.1016/s0025-3227(99)00057-2), 1999.
- 1060 Dugdale, R. C.: Chemical oceanography and primary productivity in upwelling regions,  
1061 *Geoforum*, 3, 47–61, [https://doi.org/10.1016/0016-7185\(72\)90085-1](https://doi.org/10.1016/0016-7185(72)90085-1), 1972.
- 1062 Falkowski, P. G.: Evolution of the nitrogen cycle and its influence on the biological  
1063 sequestration of CO<sub>2</sub> in the ocean, *Nature*, 387, 272–275, <https://doi.org/10.1038/387272a0>,  
1064 1997.
- 1065 Findlater, J.: A major low-level air current near the Indian Ocean during the northern summer,  
1066 *Q. J. R. Meteorol. Soc.*, 95, 362–380, 1969.

1067 Flower, B. P. and Kennett, J. P.: The middle Miocene climatic transition: East Antarctic ice  
1068 sheet development, deep ocean circulation and global carbon cycling, *Palaeogeogr.*  
1069 *Palaeoclimatol. Palaeoecol.*, 108, 537–555, [https://doi.org/10.1016/0031-0182\(94\)90251-8](https://doi.org/10.1016/0031-0182(94)90251-8),  
1070 1994.

1071 Frigola, A., Prange, M., and Schulz, M.: Boundary conditions for the Middle Miocene  
1072 Climate Transition (MMCT v1.0), *Geosci. Model Dev.*, 11, 1607–1626,  
1073 <https://doi.org/10.5194/gmd-11-1607-2018>, 2018.

1074 Gadgil, S.: The monsoon system: Land–sea breeze or the ITCZ?, *Journal of Earth System*  
1075 *Science*, 127, 1–29, <https://doi.org/10.1007/s12040-017-0916-x>, 2018.

1076 Garcia, Weathers, K., Paver, C. R., Smolyar, I., Boyer, T. P., Locarnini, R. A., Zweng, M. M.,  
1077 Mishonov, A. V., Baranova, O. K., Seidov, D., and Reagan, J. R.: World Ocean Atlas 2018  
1078 Volume 3: Dissolved Oxygen, Apparent Oxygen Utilization, and Oxygen Saturation, NOAA  
1079 Atlas NESDIS 83, 38 pp., 2018.

1080 Garnesson, P., Mangin, A., d’Andon, O. F., Demaria, J., and Bretagnon, M.: The CMEMS  
1081 GlobColour chlorophyll a product based on satellite observation: multi-sensor merging and  
1082 flagging strategies, *Ocean Sci.*, 15, 819–830, <https://doi.org/10.5194/os-15-819-2019>, 2019.

1083 Gaye, B., Böll, A., Segsneider, J., Burdanowitz, N., Emeis, K.-C., Ramaswamy, V.,  
1084 Lahajnar, N., Lückge, A., and Rixen, T.: Glacial–interglacial changes and Holocene variations  
1085 in Arabian Sea denitrification, *Biogeosciences*, 15, 507–527, [https://doi.org/10.5194/bg-15-](https://doi.org/10.5194/bg-15-507-2018)  
1086 [507-2018](https://doi.org/10.5194/bg-15-507-2018), 2018.

1087 Gibbs, S., Shackleton, N., and Young, J.: Orbitally forced climate signals in mid-Pliocene  
1088 nannofossil assemblages, *Mar. Micropaleontol.*, 51, 39–56,  
1089 <https://doi.org/10.1016/j.marmicro.2003.09.002>, 2004a.

1090 Gibbs, S. J., Shackleton, N. J., and Young, J. R.: Identification of dissolution patterns in  
1091 nannofossil assemblages: A high-resolution comparison of synchronous records from Ceara  
1092 Rise, ODP Leg 154, *Paleoceanography*, 19, 1–12, <https://doi.org/10.1029/2003pa000958>,  
1093 2004b.

1094 Gibbs, S. J., Young, J. R., Bralower, T. J., and Shackleton, N. J.: Nannofossil evolutionary  
1095 events in the mid-Pliocene: an assessment of the degree of synchrony in the extinctions of  
1096 *Reticulofenestra pseudumbilicus* and *Sphenolithus abies*, *Palaeogeogr. Palaeoclimatol.*  
1097 *Palaeoecol.*, 217, 155–172, <https://doi.org/10.1016/j.palaeo.2004.11.005>, 2005.

1098 Gohin, F.: Annual cycles of chlorophyll-*a*, non-algal suspended particulate matter, and  
1099 turbidity observed from space and in-situ in coastal waters, *Ocean Sci.*, 7, 705–732,  
1100 <https://doi.org/10.5194/os-7-705-2011>, 2011.

1101 Gourlan, A. T., Meynadier, L., and Allègre, C. J.: Tectonically driven changes in the Indian  
1102 Ocean circulation over the last 25 Ma: Neodymium isotope evidence, *Earth Planet. Sci. Lett.*,  
1103 267, 353–364, <https://doi.org/10.1016/j.epsl.2007.11.054>, 2008.

1104 Groeneveld, J., Henderiks, J., Renema, W., McHugh, C. M., DeVleeschouwer, D.,  
1105 Christensen, B. A., Fulthorpe, C. S., Reuning, L., Gallagher, S. J., Bogus, K., Auer, G.,  
1106 Ishiwa, T., and Scientists, E. 356: Australian shelf sediments reveal shifts in Miocene

- 1107 Southern Hemisphere westerlies, *Sci. Adv.*, 3, 1–8, <https://doi.org/10.1126/sciadv.1602567>,  
1108 2017.
- 1109 Guieu, C., Azhar, M. A., Aumont, O., Mahowald, N., Levy, M., Ethé, C., and Lachkar, Z.:  
1110 Major Impact of Dust Deposition on the Productivity of the Arabian Sea, *Geophys Res Lett*,  
1111 46, 6736–6744, <https://doi.org/10.1029/2019gl082770>, 2019.
- 1112 Gupta, A. K. and Thomas, E.: Initiation of Northern Hemisphere glaciation and strengthening  
1113 of the northeast Indian monsoon: Ocean Drilling Program Site 758, eastern equatorial Indian  
1114 Ocean, *Geology*, 31, 47–50, [https://doi.org/10.1130/0091-  
1115 7613\(2003\)031<0047:ionhga>2.0.co;2](https://doi.org/10.1130/0091-7613(2003)031<0047:ionhga>2.0.co;2), 2003.
- 1116 Gupta, A. K., Singh, R. K., Joseph, S., and Thomas, E.: Indian Ocean high-productivity event  
1117 (10–8 Ma): Linked to global cooling or to the initiation of the Indian monsoons?, *Geology*,  
1118 32, 753–756, <https://doi.org/10.1130/g20662.1>, 2004.
- 1119 Gupta, A. K., Yuvaraja, A., Prakasam, M., Clemens, S. C., and Velu, A.: Evolution of the  
1120 South Asian monsoon wind system since the late Middle Miocene, *Palaeogeogr.*  
1121 *Palaeoclimatol. Palaeoecol.*, 438, 160–167, <https://doi.org/10.1016/j.palaeo.2015.08.006>,  
1122 2015.
- 1123 Hall, R.: Sundaland and Wallacea: Geology, plate tectonics and palaeogeography, edited by:  
1124 Gower, D., Johnson, Kenneth, Richardson, James, Rosen, Brian, Ruber, Lukas, and Williams,  
1125 S., Cambridge University Press, 32–78, <https://doi.org/10.1017/cbo9780511735882.005>,  
1126 2012.
- 1127 Hammer, Ø. and Harper, D. A. T.: *Paleontological Data Analysis*, 1st ed., Blackwell  
1128 Publishing Ltd, 2006.
- 1129 Hammer, Ø., Harper, D. A. T., and Ryan, P. D.: PAST: paleontological statistics software  
1130 package for education and data analysis, *Palaeontol. Electron.*, 4, 1–9, 2001.
- 1131 Haq, B. U.: Biogeographic history of Miocene calcareous nannoplankton and  
1132 paleoceanography of the Atlantic Ocean, *Micropaleontology*, 26, 414–443, 1980.
- 1133 Haq, B. U. and Lohmann, G. P.: Early Cenozoic calcareous nannoplankton biogeography of  
1134 the Atlantic Ocean, *Mar. Micropaleontol.*, 1, 119–194, 1976.
- 1135 Harzhauser, M., Kroh, A., Mandic, O., Piller, W. E., Göhlich, U., Reuter, M., and Berning,  
1136 B.: Biogeographic responses to geodynamics: A key study all around the Oligo–Miocene  
1137 Tethyan Seaway, Special Issue: Phylogenetic Symposium 48th Phylogenetic Symposium on  
1138 Historical Biogeography, 246, 241–256, <https://doi.org/10.1016/j.jcz.2007.05.001>, 2007.
- 1139 Holbourn, A., Kuhnt, W., Lyle, M., Schneider, L., Romero, O., and Andersen, N.: Middle  
1140 Miocene climate cooling linked to intensification of eastern equatorial Pacific upwelling,  
1141 *Geology*, 42, 19–22, <https://doi.org/10.1130/g34890.1>, 2014.
- 1142 Holbourn, A., Kuhnt, W., Kochhann, K. G. D., Andersen, N., and Meier, K. J. S.: Global  
1143 perturbation of the carbon cycle at the onset of the Miocene Climatic Optimum, *Geology*, 43,  
1144 123–126, <https://doi.org/10.1130/g36317.1>, 2015.

- 1145 Holbourn, A. E., Kuhnt, W., Clemens, S. C., Kochhann, K. G. D., Jöhnck, J., Lübbers, J., and  
1146 Andersen, N.: Late Miocene climate cooling and intensification of southeast Asian winter  
1147 monsoon, *Nat. Commun.*, 9, 365, <https://doi.org/10.1038/s41467-018-03950-1>, 2018.
- 1148 Honjo, S., Dymond, J., Prell, W., and Ittekkot, V.: Monsoon-controlled export fluxes to the  
1149 interior of the Arabian Sea, *Deep Sea Res. Part II Top. Stud. Oceanogr.*, 46, 1859–1902,  
1150 [https://doi.org/10.1016/s0967-0645\(99\)00047-8](https://doi.org/10.1016/s0967-0645(99)00047-8), 1999.
- 1151 House, M. A., Rea, D. K., and Janecek, T. R.: Proceedings of the Ocean Drilling Program,  
1152 121 Scientific Results, vol. 121, edited by: Weissel, J., Peirce, J., Taylor, E., and Alt, J., 211–  
1153 218, <https://doi.org/10.2973/odp.proc.sr.121.133.1991>, 1991.
- 1154 Hu, C., Lee, Z., and Franz, B.: Chlorophyll algorithms for oligotrophic oceans: A novel  
1155 approach based on three-band reflectance difference, *J Geophys Res Oceans*, 117,  
1156 <https://doi.org/10.1029/2011jc007395>, 2012.
- 1157 Huang, Y., Clemens, S. C., Liu, W., Wang, Y., and Prell, W. L.: Large-scale hydrological  
1158 change drove the late Miocene C4 plant expansion in the Himalayan foreland and Arabian  
1159 Peninsula, *Geology*, 35, 531–534, 2007a.
- 1160 Huang, Y., Clemens, S. C., Liu, W., Wang, Y., and Prell, W. L.: Large-scale hydrological  
1161 change drove the late Miocene C4 plant expansion in the Himalayan foreland and Arabian  
1162 Peninsula, *Geology*, 35, 531–534, <https://doi.org/10.1130/g23666a.1>, 2007b.
- 1163 Hutchins, D. A. and Bruland, K. W.: Iron-limited diatom growth and Si:N uptake ratios in a  
1164 coastal upwelling regime, *Nature*, 393, 561–564, <https://doi.org/10.1038/31203>, 1998.
- 1165 Imai, R., Farida, M., Sato, T., and Iryu, Y.: Evidence for eutrophication in the northwestern  
1166 Pacific and eastern Indian oceans during the Miocene to Pleistocene based on the nannofossil  
1167 accumulation rate, Discoaster abundance, and coccolith size distribution of *Reticulofenestra*,  
1168 *Mar. Micropaleontol.*, 116, 15–27, <https://doi.org/10.1016/j.marmicro.2015.01.001>, 2015.
- 1169 Imai, R., Sato, T., and Iryu, Y.: Calcareous nannofossil assemblages of the upper Miocene to  
1170 Pliocene Shimajiri Group on Okinawa-jima, Ryukyu Islands, southwestern Japan, *J. Asian  
1171 Earth Sci.*, 135, 16–24, <https://doi.org/10.1016/j.jseaes.2016.12.011>, 2017.
- 1172 Itou, M., Ono, T., Oba, T., and Noriki, S.: Isotopic composition and morphology of living  
1173 *Globorotalia scitula*: a new proxy of sub-intermediate ocean carbonate chemistry?, *Mar.  
1174 Micropaleontol.*, 42, 189–210, [https://doi.org/10.1016/s0377-8398\(01\)00015-9](https://doi.org/10.1016/s0377-8398(01)00015-9), 2001.
- 1175 Jatiningrum, R. S. and Sato, T.: Sea-Surface Dynamics Changes in the Subpolar North  
1176 Atlantic Ocean (IODP Site U1314) during Late Pliocene Climate Transition Based on  
1177 Calcareous Nannofossil Observation, *Open J. Geol.*, 07, 1538–1551,  
1178 <https://doi.org/10.4236/ojg.2017.710103>, 2017.
- 1179 Karatsolis, B.-T. and Henderiks, J.: Late Neogene nannofossil assemblages as tracers of ocean  
1180 circulation and paleoproductivity over the NW Australian shelf, *Clim Past*, 19, 765–786,  
1181 <https://doi.org/10.5194/cp-19-765-2023>, 2023.



- 1182 Keller, G. and Barron, J. A.: Paleocceanographic implications of Miocene deep-sea hiatuses,  
1183 Gsa Bulletin, 94, 590–613, [https://doi.org/10.1130/0016-7606\(1983\)94<590:piomdh>2.0.co;2](https://doi.org/10.1130/0016-7606(1983)94<590:piomdh>2.0.co;2), 1983.
- 1185 Kennett, J. P. and Srinivasan, M. S.: Neogene Planktonic Foraminifera: A Phylogenetic Atlas,  
1186 Hutchinson Ross; Distributed by worldwide by Van Nostrand Reinhold, Stroudsburg, PA, 265  
1187 pp. pp., 1983.
- 1188 Krapivin, V. F. and Varotsos, C. A.: Modelling the CO<sub>2</sub> atmosphere-ocean flux in the  
1189 upwelling zones using radiative transfer tools, J. Atmos. Sol.-Terr. Phys., 150, 47–54,  
1190 <https://doi.org/10.1016/j.jastp.2016.10.015>, 2016.
- 1191 Kroon, D., Steens, T. N. F., and Troelstra, S. R.: Proceedings of the Ocean Drilling Program,  
1192 117 Scientific Results, Proc Ocean Drill Program, 117,  
1193 <https://doi.org/10.2973/odp.proc.sr.117.126.1991>, 1991.
- 1194 Kuhnt, W., Holbourn, A., Xu, J., Opdyke, B., Deckker, P. D., Röhl, U., and Mudelsee, M.:  
1195 Southern Hemisphere control on Australian monsoon variability during the late deglaciation  
1196 and Holocene, Nat. Commun., 6, 5916, <https://doi.org/10.1038/ncomms6916>, 2015.
- 1197 Kunkelova, T., Crocker, A. J., Jewell, A. M., Breeze, P. S., Drake, N. A., Cooper, M. J.,  
1198 Milton, J. A., Hennen, M., Shahgedanova, M., Petraglia, M., and Wilson, P. A.: Dust sources  
1199 in Westernmost Asia have a different geochemical fingerprint to those in the Sahara,  
1200 Quaternary Sci Rev, 294, 107717, <https://doi.org/10.1016/j.quascirev.2022.107717>, 2022.
- 1201 Lahiri, S. P. and Vissa, N. K.: Assessment of Indian Ocean upwelling changes and its  
1202 relationship with the Indian monsoon, Global Planet Change, 208, 103729,  
1203 <https://doi.org/10.1016/j.gloplacha.2021.103729>, 2022.
- 1204 Laufkötter, C. and Gruber, N.: Will marine productivity wane?, Science, 359, 1103–1104,  
1205 <https://doi.org/10.1126/science.aat0795>, 2018.
- 1206 Lee, C., Murray, D. W., Barber, R. T., Buesseler, K. O., Dymond, J., Hedges, J. I., Honjo, S.,  
1207 Manganini, S. J., Marra, J., Moser, C., Peterson, M. L., Prell, W. L., and Wakeham, S. G.:  
1208 Particulate organic carbon fluxes: compilation of results from the 1995 US JGOFS Arabian  
1209 Sea Process Study, Deep Sea Res. Part II Top. Stud. Oceanogr., 45, 2489–2501,  
1210 [https://doi.org/10.1016/s0967-0645\(98\)00079-4](https://doi.org/10.1016/s0967-0645(98)00079-4), 1998.
- 1211 LeHouedec, S., Meynadier, L., and Allègre, C. J.: Nd isotope systematics on ODP Sites 756  
1212 and 762 sediments reveal major volcanic, oceanic and climatic changes in South Indian Ocean  
1213 over the last 35Ma, Earth Planet. Sci. Lett., 327–328, 29–38,  
1214 <https://doi.org/10.1016/j.epsl.2012.01.019>, 2012.
- 1215 Lessa, D., Morard, R., Jonkers, L., Venancio, I. M., Reuter, R., Baumeister, A., Albuquerque,  
1216 A. L., and Kucera, M.: Distribution of planktonic foraminifera in the subtropical South  
1217 Atlantic: depth hierarchy of controlling factors, Biogeosciences, 17, 4313–4342,  
1218 <https://doi.org/10.5194/bg-17-4313-2020>, 2020.
- 1219 Ling, A., Eberli, G. P., Swart, P. K., Reolid, J., Stainbank, S., Rüggeberg, A., and Betzler, C.:  
1220 Middle Miocene platform drowning in the Maldives associated with monsoon-related

- 1221 intensification of currents, *Palaeogeogr Palaeoclim Palaeoecol*, 567, 110275,  
1222 <https://doi.org/10.1016/j.palaeo.2021.110275>, 2021.
- 1223 Litchman, E., Klausmeier, C. A., Miller, J. R., Schofield, O. M., and Falkowski, P. G.: Multi-  
1224 nutrient, multi-group model of present and future oceanic phytoplankton communities,  
1225 *Biogeosciences*, 3, 585–606, <https://doi.org/10.5194/bg-3-585-2006>, 2006.
- 1226 Lohmann, G. P. and Carlson, J. J.: Oceanographic significance of Pacific Late Miocene  
1227 calcareous nannoplankton, *Mar. Micropaleontol.*, 6, 553–579, 1981.
- 1228 Lübbers, J., Kuhnt, W., Holbourn, A. E., Bolton, C. T., Gray, E., Usui, Y., Kochhann, K. G.  
1229 D., Beil, S., and Andersen, N.: The middle to late Miocene “Carbonate Crash” in the  
1230 equatorial Indian Ocean, *Paleoceanogr. Paleoclimatol.*, 0, 2018PA003482,  
1231 <https://doi.org/10.1029/2018pa003482>, 2019.
- 1232 Madhupratap, M., Kumar, S. P., Bhattathiri, P. M. A., Kumar, M. D., Raghukumar, S., Nair,  
1233 K. K. C., and Ramaiah, N.: Mechanism of the biological response to winter cooling in the  
1234 northeastern Arabian Sea, *Nature*, 384, 549–552, <https://doi.org/10.1038/384549a0>, 1996.
- 1235 Majewski, W.: Water-depth distribution of Miocene planktonic foraminifera from ODP Site  
1236 744, southern Indian Ocean, *J Foramin Res*, 33, 144–154, <https://doi.org/10.2113/0330144>,  
1237 2003.
- 1238 McCreary, J. P., Yu, Z., Hood, R. R., Vinayachandran, P. N., Furue, R., Ishida, A., and  
1239 Richards, K. J.: Dynamics of the Indian-Ocean oxygen minimum zones, *Prog. Oceanogr.*,  
1240 112–113, 15–37, <https://doi.org/10.1016/j.pocean.2013.03.002>, 2013.
- 1241 Meisel, S., Struck, U., and Emeis, K.: Nutrient dynamics and oceanographic features in the  
1242 central Namibian upwelling region as reflected in  $\delta^{15}\text{N}$ -signals of suspended matter and  
1243 surface sediments, *Foss Rec*, 14, 153–169, <https://doi.org/10.1002/mmng.201100005>, 2011.
- 1244 Mikaelyan, A. S., Pautova, L. A., Chasovnikov, V. K., Mosharov, S. A., and Silkin, V. A.:  
1245 Alternation of diatoms and coccolithophores in the north-eastern Black Sea: a response to  
1246 nutrient changes, *Hydrobiologia*, 755, 89–105, <https://doi.org/10.1007/s10750-015-2219-z>,  
1247 2015.
- 1248 Miller, K. G., Browning, J. V., Schmelz, W. J., Kopp, R. E., Mountain, G. S., and Wright, J.  
1249 D.: Cenozoic sea-level and cryospheric evolution from deep-sea geochemical and continental  
1250 margin records, *Sci Adv*, 6, eaaz1346, 2020.
- 1251 Millero, F. J.: The Marine Inorganic Carbon Cycle, *Chem Rev*, 107, 308–341,  
1252 <https://doi.org/10.1021/cr0503557>, 2007.
- 1253 Moore, C. M., Mills, M. M., Arrigo, K. R., Berman-Frank, I., Bopp, L., Boyd, P. W.,  
1254 Galbraith, E. D., Geider, R. J., Guieu, C., Jaccard, S. L., Jickells, T. D., Roche, J. L., Lenton,  
1255 T. M., Mahowald, N. M., Marañón, E., Marinov, I., Moore, J. K., Nakatsuka, T., Oschlies, A.,  
1256 Saito, M. A., Thingstad, T. F., Tsuda, A., and Ulloa, O.: Processes and patterns of oceanic  
1257 nutrient limitation, 6, 701–710, <https://doi.org/10.1038/ngeo1765>, 2013.
- 1258 Moore, J. K., Fu, W., Primeau, F., Britten, G. L., Lindsay, K., Long, M., Doney, S. C.,  
1259 Mahowald, N., Hoffman, F., and Randerson, J. T.: Sustained climate warming drives

- 1260 declining marine biological productivity, *Science*, 359, 1139–1143,  
1261 <https://doi.org/10.1126/science.aao6379>, 2018.
- 1262 Morrison, J. M., Codispoti, L. A., Gaurin, S., Jones, B., Manghnani, V., and Zheng, Z.:  
1263 Seasonal variation of hydrographic and nutrient fields during the US JGOFS Arabian Sea  
1264 Process Study, *Deep Sea Res. Part II Top. Stud. Oceanogr.*, 45, 2053–2101,  
1265 [https://doi.org/10.1016/s0967-0645\(98\)00063-0](https://doi.org/10.1016/s0967-0645(98)00063-0), 1998.
- 1266 Munz, P. M., Siccha, M., Lückge, A., Böll, A., Kucera, M., and Schulz, H.: Decadal-  
1267 resolution record of winter monsoon intensity over the last two millennia from planktic  
1268 foraminiferal assemblages in the northeastern Arabian Sea, *The Holocene*,  
1269 0959683615591357, <https://doi.org/10.1177/0959683615591357>, 2015.
- 1270 Munz, P. M., Steinke, S., Böll, A., Lückge, A., Groeneveld, J., Kucera, M., and Schulz, H.:  
1271 Decadal resolution record of Oman upwelling indicates solar forcing of the Indian summer  
1272 monsoon (9–6 ka), *Clim. Past.*, 13, 491–509, <https://doi.org/10.5194/cp-13-491-2017>, 2017.
- 1273 Naik, D. K., Saraswat, R., Lea, D. W., Kurtarkar, S. R., and Mackensen, A.: Last glacial-  
1274 interglacial productivity and associated changes in the eastern Arabian Sea, *Palaeogeogr*  
1275 *Palaeoclim Palaeoecol.*, 483, 147–156, <https://doi.org/10.1016/j.palaeo.2016.07.014>, 2017.
- 1276 Negri, A. and Villa, G.: Calcareous nannofossil biostratigraphy, biochronology and  
1277 paleoecology at the Tortonian/Messinian boundary of the Faneromeni section (Crete),  
1278 *Palaeogeogr. Palaeoclimatol. Palaeoecol.*, 156, 195–209, 2000.
- 1279 Nigrini, C.: Composition and Biostratigraphy of Radiolarian Assemblages from an Area of  
1280 Upwelling (Northwestern Arabian Sea, Leg 117), in: *Proceedings of the Ocean Drilling*  
1281 *Program, 117 Scientific Results*, vol. 117, edited by: Prell, W. J. and Niitsuma, N., 89–126,  
1282 <https://doi.org/10.2973/odp.proc.sr.117.132.1991>, 1991.
- 1283 Nikolaev, S. D., Oskina, N. S., Blyum, N. S., and Bubenshchikova, N. V.: Neogene–  
1284 Quaternary variations of the ‘Pole–Equator’ temperature gradient of the surface oceanic  
1285 waters in the North Atlantic and North Pacific, *Global Planet Change*, 18, 85–111,  
1286 [https://doi.org/10.1016/s0921-8181\(98\)00009-5](https://doi.org/10.1016/s0921-8181(98)00009-5), 1998.
- 1287 Paasche, E.: Roles of nitrogen and phosphorus in coccolith formation in *Emiliania huxleyi*  
1288 (*Prymnesiophyceae*), *Eur J Phycol.*, 33, 33–42,  
1289 <https://doi.org/10.1080/09670269810001736513>, 1998.
- 1290 Paerl, H. W.: Why does N-limitation persist in the world’s marine waters?, *Mar. Chem.*, 206,  
1291 1–6, <https://doi.org/10.1016/j.marchem.2018.09.001>, 2018.
- 1292 Pearson, P. N. and Shackleton, N. J.: Neogene multispecies planktonic foraminifer stable  
1293 isotope record, Site 871, Limalok Guyot, in: *Proceedings of the Ocean Drilling Program, 144*  
1294 *Scientific Results*, edited by: Haggerty, J. A., Premoli-Silva, I., Rack, F., and McNutt, M. K.,  
1295 <https://doi.org/10.2973/odp.proc.sr.144.054.1995>, 1995.
- 1296 Pearson, P. N. and Wade, B. S.: Taxonomy and stable isotope paleoecology of well-preserved  
1297 planktonic foraminifera from the uppermost oligocene of Trinidad, *J Foramin Res.*, 39, 191–  
1298 217, <https://doi.org/10.2113/gsjfr.39.3.191>, 2009.

- 1299 Perch-Nielsen, K.: Cenozoic Calcareous Nanofossils, in: *Plankton Stratigraphy*, vol. 1, edited  
1300 by: Bolli, H. M., Saunders, J B, and Perch-Nielsen, K., 427–554, 1985.
- 1301 Pound, M. J., Haywood, A. M., Salzmann, U., and Riding, J. B.: Global vegetation dynamics  
1302 and latitudinal temperature gradients during the Mid to Late Miocene (15.97–5.33Ma), *Earth-*  
1303 *Sci. Rev.*, 112, 1–22, <https://doi.org/10.1016/j.earscirev.2012.02.005>, 2012.
- 1304 Pourmand, A., Marcantonio, F., Bianchi, T. S., Canuel, E. A., and Waterson, E. J.: A 28-ka  
1305 history of sea surface temperature, primary productivity and planktonic community variability  
1306 in the western Arabian Sea, *Paleoceanography*, 22, n/a-n/a,  
1307 <https://doi.org/10.1029/2007pa001502>, 2007.
- 1308 Prell, W. L., Murray, D. W., Clemens, S. C., and Anderson, D. M.: Evolution and Variability  
1309 of the Indian Ocean Summer Monsoon: Evidence from the Western Arabian Sea Drilling  
1310 Program, edited by: Duncan, R. A., Rea, D. K., Kidd, R. B., Rad, U. von, and Weissel, J. K.,  
1311 447–469, <https://doi.org/10.1029/gm070p0447>, 1992.
- 1312 Raven, J. A. and Falkowski, P. G.: Oceanic sinks for atmospheric CO<sub>2</sub>, *Plant Cell Environ*,  
1313 22, 741–755, <https://doi.org/10.1046/j.1365-3040.1999.00419.x>, 1999.
- 1314 Regenberg, M., Nielsen, S. N., Kuhnt, W., Holbourn, A., Garbe-Schönberg, D., and  
1315 Andersen, N.: Morphological, geochemical, and ecological differences of the extant  
1316 menardiform planktonic foraminifera *Globorotalia menardii* and *Globorotalia cultrata*, *Mar.*  
1317 *Micropaleontol.*, 74, 96–107, <https://doi.org/10.1016/j.marmicro.2010.01.002>, 2010.
- 1318 Reuter, M., Piller, W. E., Harzhauser, M., Kroh, A., and Bassi, D.: Termination of the  
1319 Arabian shelf sea: Stacked cyclic sedimentary patterns and timing (Oligocene/Miocene,  
1320 Oman), *Sediment Geol*, 212, 12–24, <https://doi.org/10.1016/j.sedgeo.2008.09.001>, 2008.
- 1321 Reuter, M., Piller, W. E., Harzhauser, M., Mandic, O., Berning, B., Rögl, F., Kroh, A., Aubry,  
1322 M. P., Wielandt-Schuster, U., and Hamedani, A.: The Oligo-/Miocene Qom Formation (Iran):  
1323 evidence for an early Burdigalian restriction of the Tethyan Seaway and closure of its Iranian  
1324 gateways, *International Journal of Earth Sciences*, 98, 627–650–650,  
1325 <https://doi.org/10.1007/s00531-007-0269-9>, 2009.
- 1326 Reuter, M., Kern, A. K., Harzhauser, M., Kroh, A., and Piller, W. E.: Global warming and  
1327 South Indian monsoon rainfall—lessons from the Mid-Miocene, *Gondwana Res.*, 23, 1172–  
1328 1177, <https://doi.org/10.1016/j.gr.2012.07.015>, 2013.
- 1329 Reuter, M., Bosellini, F. R., Budd, A. F., Ćorić, S., Piller, W. E., and Harzhauser, M.: High  
1330 coral reef connectivity across the Indian Ocean is revealed 6–7 Ma ago by a turbid-water  
1331 scleractinian assemblage from Tanzania (Eastern Africa), *Coral Reefs*, 38, 1023–1037,  
1332 <https://doi.org/10.1007/s00338-019-01830-8>, 2019.
- 1333 Ridgwell, A. and Zeebe, R. E.: The role of the global carbonate cycle in the regulation and  
1334 evolution of the Earth system, *Earth Planet. Sci. Lett.*, 234, 299–315,  
1335 <https://doi.org/10.1016/j.epsl.2005.03.006>, 2005.
- 1336 Rixen, T., Goyet, C., and Ittekkot, V.: Diatoms and their influence on the biologically  
1337 mediated uptake of atmospheric CO<sub>2</sub> in the Arabian Sea upwelling system, *Biogeosciences*, 3,  
1338 1–13, <https://doi.org/10.5194/bg-3-1-2006>, 2006.

- 1339 Rixen, T., Gaye, B., Emeis, K. C., and Ramaswamy, V.: The ballast effect of lithogenic  
1340 matter and its influences on the carbon fluxes in the Indian Ocean, *Biogeosciences*, 16, 485–  
1341 503, <https://doi.org/10.5194/bg-16-485-2019>, 2019a.
- 1342 Rixen, T., Gaye, B., and Emeis, K.: The Monsoon, Carbon Fluxes, and the Organic Carbon  
1343 Pump in the Northern Indian Ocean, *Prog. Oceanogr.*, 175, 24–39,  
1344 <https://doi.org/10.1016/j.pocean.2019.03.001>, 2019b.
- 1345 Rodriguez, M., Chamot-Rooke, N., Huchon, P., Fournier, M., and Delescluse, M.: The Owen  
1346 Ridge uplift in the Arabian Sea: Implications for the sedimentary record of Indian monsoon in  
1347 Late Miocene, *Earth Planet. Sci. Lett.*, 394, 1–12, <https://doi.org/10.1016/j.epsl.2014.03.011>,  
1348 2014.
- 1349 Rodriguez, M., Bourget, J., Chamot-Rooke, N., Huchon, P., Fournier, M., Delescluse, M., and  
1350 Zaragosi, S.: The Sawqirah contourite drift system in the Arabian Sea (NW Indian Ocean): A  
1351 case study of interactions between margin reactivation and contouritic processes, *Mar Geol.*,  
1352 381, 1–16, <https://doi.org/10.1016/j.margeo.2016.08.004>, 2016.
- 1353 Rögl, F.: Mediterranean and Paratethys. Facts and hypotheses of an Oligocene to Miocene  
1354 paleogeography (short overview), *Geologica Carpathica*, 50, 339–349, 1999.
- 1355 Samtleben, C.: Die Evolution der Coccolithophoriden-Gattung *Gephyrocapsa* nach Befunden  
1356 im Atlantik, *PalZ*, 54, 91–127–127, <https://doi.org/10.1007/bf02985885>, 1980.
- 1357 Sarmiento, J. L. and Gruber, N.: Ocean Biogeochemical Dynamics, 359–391,  
1358 <https://doi.org/10.2307/j.ctt3fgxqx.13>, 2013.
- 1359 Sarmiento, J. L., Gruber, N., Brzezinski, M. A., and Dunne, J. P.: High-latitude controls of  
1360 thermocline nutrients and low latitude biological productivity, *Nature*, 427, 56–60,  
1361 <https://doi.org/10.1038/nature02127>, 2004.
- 1362 Sarr, A.-C., Donnadieu, Y., Bolton, C. T., Ladant, J.-B., Licht, A., Fluteau, F., Laugié, M.,  
1363 Tardif, D., and Dupont-Nivet, G.: Neogene South Asian monsoon rainfall and wind histories  
1364 diverged due to topographic effects, *Nat Geosci*, 15, 314–319, [https://doi.org/10.1038/s41561-  
1365 022-00919-0](https://doi.org/10.1038/s41561-022-00919-0), 2022.
- 1366 Schiebel, R., Zeltner, A., Treppke, U. F., Waniek, J. J., Bollmann, J., Rixen, T., and  
1367 Hemleben, C.: Distribution of diatoms, coccolithophores and planktic foraminifers along a  
1368 trophic gradient during SW monsoon in the Arabian Sea, *Mar. Micropaleontol.*, 51, 345–371,  
1369 <https://doi.org/10.1016/j.marmicro.2004.02.001>, 2004.
- 1370 Schlitzer, R.: Ocean Data View, 2021.
- 1371 Schott, F. A. and McCreary, J. P.: The monsoon circulation of the Indian Ocean, *Prog.*  
1372 *Oceanogr.*, 51, 1–123, 2001.
- 1373 Schott, F. A., Xie, S.-P., and Jr., J. P. M.: Indian Ocean circulation and climate variability,  
1374 *Reviews of Geophysics*, 47, 3295, <https://doi.org/10.1029/2007rg000245>, 2009.

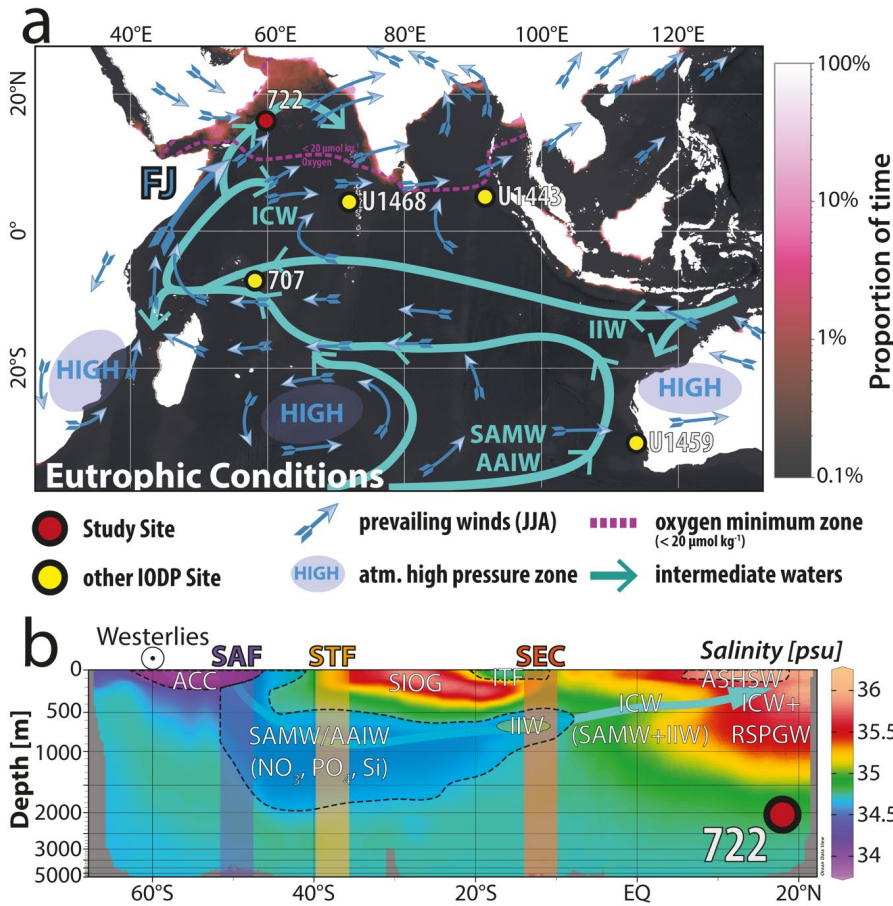
- 1375 Schubert, C. J., Villanueva, J., Calvert, S. E., Cowie, G. L., Rad, U. von, Schulz, H., Berner,  
1376 U., and Erlenkeuser, H.: Stable phytoplankton community structure in the Arabian Sea over  
1377 the past 200,000 years, *Nature*, 394, 563–566, <https://doi.org/10.1038/29047>, 1998.
- 1378 Schueth, J. D. and Bralower, T. J.: The relationship between environmental change and the  
1379 extinction of the nannoplankton Discoaster in the early Pleistocene, *Paleoceanography*, 30,  
1380 863–876, <https://doi.org/10.1002/2015pa002803>, 2015.
- 1381 Sexton, P. F. and Norris, R. D.: High latitude regulation of low latitude thermocline  
1382 ventilation and planktic foraminifer populations across glacial–interglacial cycles, *Earth*  
1383 *Planet. Sci. Lett.*, 311, 69–81, <https://doi.org/10.1016/j.epsl.2011.08.044>, 2011.
- 1384 Shimmiel, G. B.: Can sediment geochemistry record changes in coastal upwelling  
1385 palaeoproductivity? Evidence from northwest Africa and the Arabian Sea, *Geological Soc*  
1386 *Lond Special Publ*, 64, 29–46, <https://doi.org/10.1144/gsl.sp.1992.064.01.03>, 1992.
- 1387 Shipboard-Scientific-Party: Site 722, vol. 117,  
1388 <https://doi.org/10.2973/odp.proc.ir.117.107.1989>, 1989.
- 1389 Sigman, D. M. and Fripiat, F.: Nitrogen Isotopes in the Ocean, in: *Encyclopedia of Ocean*  
1390 *Sciences (Third Edition)*, edited by: Cochran, J. K., Bokuniewicz, H. J., and Yager, P. L.,  
1391 263–278, <https://doi.org/10.1016/b978-0-12-409548-9.11605-7>, 2019.
- 1392 Smart, C. W., Thomas, E., and Ramsay, A. T. S.: Middle–late Miocene benthic foraminifera  
1393 in a western equatorial Indian Ocean depth transect: Paleooceanographic implications,  
1394 *Palaeogeogr. Palaeoclimatol. Palaeoecol.*, 247, 402–420,  
1395 <https://doi.org/10.1016/j.palaeo.2006.11.003>, 2007.
- 1396 Sokal, R. R. and Rohlf, F. J.: *Biometry*, 3rd ed., W. H. Freeman and Company, 1995.
- 1397 Sosdian, S. M. and Lear, C. H.: Initiation of the Western Pacific Warm Pool at the Middle  
1398 Miocene Climate Transition?, *Paleoceanogr. Paleoclimatol.*,  
1399 <https://doi.org/10.1029/2020pa003920>, 2020.
- 1400 Spezzaferri, S.: Planktonic foraminiferal paleoclimatic implications across the Oligocene-  
1401 Miocene transition in the oceanic record (Atlantic, Indian and South Pacific), *Palaeogeogr*  
1402 *Palaeoclim Palaeoecol*, 114, 43–74, [https://doi.org/10.1016/0031-0182\(95\)00076-x](https://doi.org/10.1016/0031-0182(95)00076-x), 1995.
- 1403 Stramma, L., Johnson, G. C., Sprintall, J., and Mohrholz, V.: Expanding Oxygen-Minimum  
1404 Zones in the Tropical Oceans, *Science*, 320, 655–658,  
1405 <https://doi.org/10.1126/science.1153847>, 2008.
- 1406 Suess, E.: Particulate organic carbon flux in the oceans—surface productivity and oxygen  
1407 utilization, *Nature*, 288, 260–263, <https://doi.org/10.1038/288260a0>, 1980.
- 1408 Taucher, J., Bach, L. T., Prowe, A. E. F., Boxhammer, T., Kvale, K., and Riebesell, U.:  
1409 Enhanced silica export in a future ocean triggers global diatom decline, *Nature*, 605, 696–700,  
1410 <https://doi.org/10.1038/s41586-022-04687-0>, 2022.
- 1411 ThiDieuVu, H. and Sohrin, Y.: Diverse stoichiometry of dissolved trace metals in the Indian  
1412 Ocean, *Sci. Rep.*, 3, 1745, <https://doi.org/10.1038/srep01745>, 2013.

- 1413 Toggweiler, J. R., Druffel, E. R. M., Key, R. M., and Galbraith, E. D.: Upwelling in the  
1414 Ocean Basins North of the ACC: 1. On the Upwelling Exposed by the Surface Distribution of  
1415  $\Delta^{14}\text{C}$ , *J. Geophys. Res.: Oceans*, 124, 2591–2608, <https://doi.org/10.1029/2018jc014794>,  
1416 2019a.
- 1417 Toggweiler, J. R., Druffel, E. R. M., Key, R. M., and Galbraith, E. D.: Upwelling in the  
1418 Ocean Basins North of the ACC: 1. On the Upwelling Exposed by the Surface Distribution of  
1419  $\Delta^{14}\text{C}$ , *J. Geophys. Res.: Oceans*, 124, 2591–2608, <https://doi.org/10.1029/2018jc014794>,  
1420 2019b.
- 1421 Tomczak, M. and Godfrey, J. S.: *Hydrology of the Indian Ocean*, edited by: Tomczak, M. and  
1422 Godfrey, J. S., Daya Publishing House, 199–214, 2003.
- 1423 Tripathi, S., Tiwari, M., Lee, J., Khim, B.-K., Pandey, D. K., Clift, P. D., Kulhanek, D. K.,  
1424 Andò, S., Bendle, J. A. P., Aharonovich, S., Griffith, E. M., Gurumurthy, G. P., Hahn, A.,  
1425 Iwai, M., Kumar, A., Kumar, A. G., Liddy, H. M., Lu, H., Lyle, M. W., Mishra, R.,  
1426 Radhakrishna, T., Routledge, C. M., Saraswat, R., Saxena, R., Scardia, G., Sharma, G. K.,  
1427 Singh, A. D., Steinke, S., Suzuki, K., Tauxe, L., Xu, Z., and Yu, Z.: First evidence of  
1428 denitrification vis-à-vis monsoon in the Arabian Sea since Late Miocene, *Sci. Rep.*, 7, 43056,  
1429 <https://doi.org/10.1038/srep43056>, 2017.
- 1430 Tudhope, A. W., Lea, D. W., Shimmield, G. B., Chilcott, C. P., and Head, S.: Monsoon  
1431 Climate and Arabian Sea Coastal Upwelling Recorded in Massive Corals from Southern  
1432 Oman, *Palaios*, 11, 347, <https://doi.org/10.2307/3515245>, 1996.
- 1433 Ustick, L. J., Larkin, A. A., Garcia, C. A., Garcia, N. S., Brock, M. L., Lee, J. A., Wiseman,  
1434 N. A., Moore, J. K., and Martiny, A. C.: Metagenomic analysis reveals global-scale patterns  
1435 of ocean nutrient limitation, *Science*, 372, 287–291, <https://doi.org/10.1126/science.abc6301>,  
1436 2021.
- 1437 Villa, G., Fioroni, C., Pea, L., Bohaty, S., and Persico, D.: Middle Eocene–late Oligocene  
1438 climate variability: Calcareous nannofossil response at Kerguelen Plateau, Site 748, Mar.  
1439 *Micropaleontol.*, 69, 173–192, <https://doi.org/10.1016/j.marmicro.2008.07.006>, 2008.
- 1440 Volk, T. and Hoffert, M. I.: Ocean Carbon Pumps: Analysis of Relative Strengths and  
1441 Efficiencies in Ocean-Driven Atmospheric  $\text{CO}_2$  Changes, in: *The Carbon Cycle and  
1442 Atmospheric  $\text{CO}_2$ : Natural Variations Archean to Present*, vol. 32, edited by: Sundquist, E. T.  
1443 and Broecker, W. S., 99–110, <https://doi.org/10.1029/gm032p0099>, 1985.
- 1444 Wade, B. S. and Bown, P. R.: Calcareous nannofossils in extreme environments: The  
1445 Messinian Salinity Crisis, Polemi Basin, Cyprus, *Palaeogeogr. Palaeoclimatol. Palaeoecol.*,  
1446 233, 271–286, <https://doi.org/10.1016/j.palaeo.2005.10.007>, 2006.
- 1447 Wang, D., Gouhier, T. C., Menge, B. A., and Ganguly, A. R.: Intensification and spatial  
1448 homogenization of coastal upwelling under climate change, *Nature*, 518, 390–394,  
1449 <https://doi.org/10.1038/nature14235>, 2015.
- 1450 Wei, W. and Wise, S. W.: Biogeographic gradients of middle Eocene-Oligocene calcareous  
1451 nannoplankton in the South Atlantic Ocean, *Palaeogeogr. Palaeoclimatol. Palaeoecol.*, 79, 29–  
1452 61, 1990.

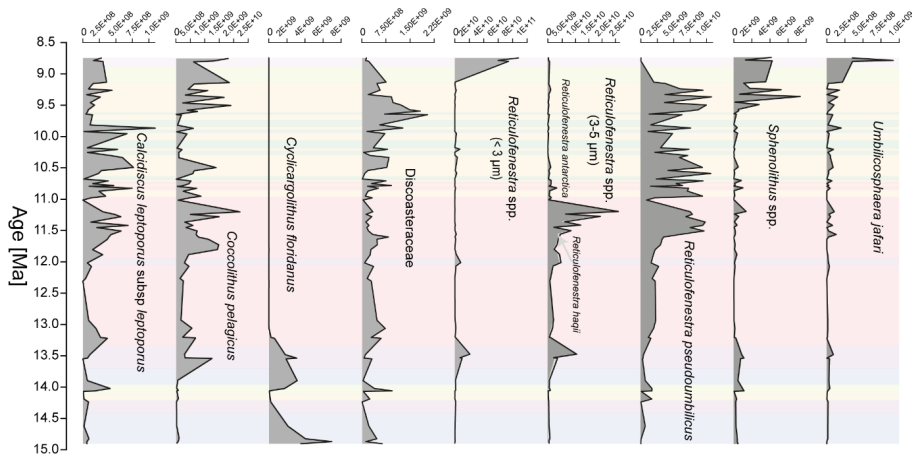


- 1453 Westerhold, T., Marwan, N., Drury, A. J., Liebrand, D., Agnini, C., Anagnostou, E., Barnet, J.  
 1454 S. K., Bohaty, S. M., Vleeschouwer, D. D., Florindo, F., Frederichs, T., Hodell, D. A.,  
 1455 Holbourn, A. E., Kroon, D., Lauretano, V., Littler, K., Lourens, L. J., Lyle, M., Pälike, H.,  
 1456 Röhl, U., Tian, J., Wilkens, R. H., Wilson, P. A., and Zachos, J. C.: An astronomically dated  
 1457 record of Earth's climate and its predictability over the last 66 million years, *Science*, 369,  
 1458 1383–1387, <https://doi.org/10.1126/science.aba6853>, 2020.
- 1459 Woodruff, F. and Savin, S. M.: Miocene deepwater oceanography, *Paleoceanography*, 4, 87–  
 1460 140, <https://doi.org/10.1029/pa004i001p00087>, 1989.
- 1461 Woodward, E. M. S., Rees, A. P., and Stephens, J. A.: The influence of the south-west  
 1462 monsoon upon the nutrient biogeochemistry of the Arabian Sea, *Deep Sea Res. Part II Top.*  
 1463 *Stud. Oceanogr.*, 46, 571–591, [https://doi.org/10.1016/s0967-0645\(98\)00118-0](https://doi.org/10.1016/s0967-0645(98)00118-0), 1999.
- 1464 Yang, X., Groeneveld, J., Jian, Z., Steinke, S., and Giosan, L.: Middle Miocene Intensification  
 1465 of South Asian Monsoonal Rainfall, *Paleoceanogr. Paleoclimatol.*, 35,  
 1466 <https://doi.org/10.1029/2020pa003853>, 2020.
- 1467 Yao, Z., Shi, X., Guo, Z., Li, X., Nath, B. N., Betzler, C., Zhang, H., Lindhorst, S., and  
 1468 Miriyala, P.: Weakening of the South Asian summer monsoon linked to interhemispheric ice-  
 1469 sheet growth since 12 Ma, *Nat. Commun.*, 14, 829, [https://doi.org/10.1038/s41467-023-](https://doi.org/10.1038/s41467-023-36537-6)  
 1470 [36537-6](https://doi.org/10.1038/s41467-023-36537-6), 2023.
- 1471 You, Y.: Seasonal variations of thermocline circulation and ventilation in the Indian Ocean, *J.*  
 1472 *Geophys. Res.: Oceans*, 102, 10391–10422, <https://doi.org/10.1029/96jc03600>, 1997.
- 1473 You, Y.: Intermediate water circulation and ventilation of the Indian Ocean derived from  
 1474 water-mass contributions, 1 January 1998.
- 1475 You, Y. and Tomczak, M.: Thermocline circulation and ventilation in the Indian Ocean  
 1476 derived from water mass analysis, *Deep Sea Res. Part : Oceanogr. Res. Pap.*, 40, 13–56,  
 1477 [https://doi.org/10.1016/0967-0637\(93\)90052-5](https://doi.org/10.1016/0967-0637(93)90052-5), 1993.
- 1478 Young, J.: Size variation of Neogene Reticulofenestra coccoliths from Indian Ocean DSDP  
 1479 Cores, *J Micropalaeontol*, 9, 71–85, <https://doi.org/10.1144/jm.9.1.71>, 1990.
- 1480 Young, J. R.: Neogene, in: *Calcareous Nannofossil Biostratigraphy*, edited by: Bown, P. R.,  
 1481 225–265, 1998.
- 1482 Nannotax 3: <http://www.mikrotax.org/Nannotax3/>, last access: 24 July 2023.
- 1483 Zhang, Z., Ramstein, G., Schuster, M., Li, C., Contoux, C., and Yan, Q.: Aridification of the  
 1484 Sahara desert caused by Tethys Sea shrinkage during the Late Miocene, *Nature*, 513, 401–  
 1485 404, <https://doi.org/10.1038/nature13705>, 2014.
- 1486 Zhuang, G., Pagani, M., and Zhang, Y. G.: Monsoonal upwelling in the western Arabian Sea  
 1487 since the middle Miocene, *Geology*, 45, 655–658, <https://doi.org/10.1130/g39013.1>, 2017.
- 1488 Zweng, M. M., Reagan, J. R., Seidov, D., Boyer, T. P., Locarnini, M. M., Garcia, H. E.,  
 1489 Mishonov, A. V., Baranova, O. K., Weathers, K. W., Paver, C. R., and Smolyar, I.: *World*  
 1490 *ocean atlas 2018, Volume 2: Salinity*, edited by: Mishonov, A., 50 pp., 2019.





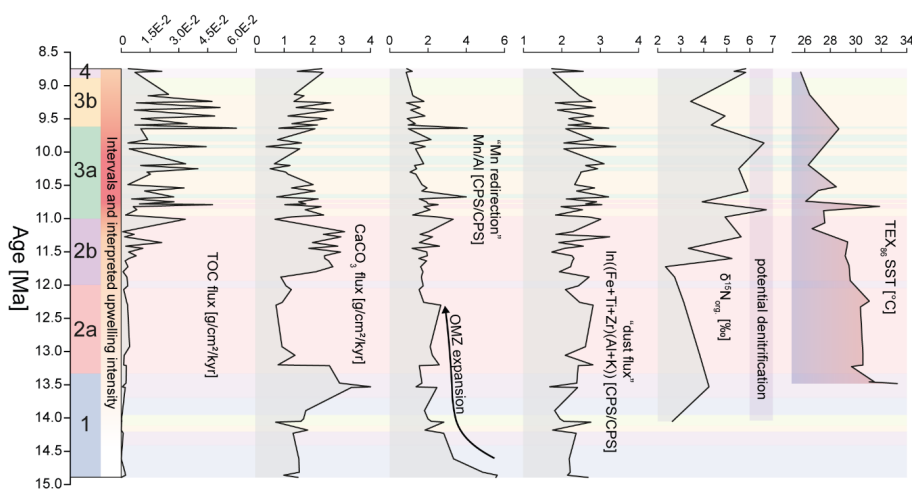
1493 **Figure 1:** a) Location map showing the study site ODP Site 722 and IODP Site U1468 and the prevalent summertime  
 1494 wind patterns following Bialik et al. (2020a). Generalized flow flow-paths of dominant intermediate waters of the Indian  
 1495 Ocean follow You (1998) and Böning (2009). The present-day extent of the oxygen minimum zone is shown as a pink  
 1496 dashed line denoting oxygen concentrations < 20 μmol kg<sup>-1</sup> at a water depth of 200 m (McCreary et al., 2013; Garcia et  
 1497 al., 2018). Eutrophication (magenta shading) data was provided by the E.U. Copernicus Marine Service Information  
 1498 using the Global Ocean Colour (Copernicus-GlobColour), Bio-Geo-Chemical, L4 (monthly and interpolated) from  
 1499 Satellite Observations (1997-ongoing); <https://doi.org/10.48670/moi-00281>. Shading represents gap-filled daily  
 1500 Chlorophyll-a product of Copernicus GLobColour L4 (Gohin, 2011; Hu et al., 2012; Garnesson et al., 2019) and  
 1501 indicates the proportion of time spent in eutrophic conditions in the region, based on the proportion of days (1998-2022)  
 1502 where Chlorophyll-a concentration exceeded a threshold of 7.3 mg m<sup>-3</sup> (derived from Carlson, 1977). The python code  
 1503 used to generate the base map is available in the supplementary material. b) Salinity profile generated based on the  
 1504 world Ocean Atlas 2018 salinity data (Zweng et al., 2019) through the Indian Ocean from 65°S to 20°N. The plot was  
 1505 generated using Ocean Data View (Schlitzer, 2021). Water masses are differentiated based on their salinity signature  
 1506 outlined with dashed lines and labeled. Furthermore major frontal systems and currents are also indicated.  
 1507 Abbreviations: Antarctic Intermediate Water (AAIW), Antarctic Circumpolar Current (ACC), Arabian Sea High  
 1508 Salinity Water (ASHSW), Indian Central Water (ICW), Indonesian Intermediate Water (IIW), Red Sea/Persian Gulf  
 1509 Water (RSPGW), sub-Antarctic Mode Water (SAMW), Southern Indian Ocean Gyre (SIOG),



1511

1512 **Figure 2:** Abundance data of key nanofossil taxa presented as numbers per gram of carbonate over the study interval  
 1513 following the methods of Bordiga et al. (2015). The used age model is based on Bialik et al. (2020a). Medium-sized  
 1514 reticulofenestrads are separated into morphotypes with an open central area (Reticulofenestra haqii) and a closed  
 1515 central area (R. antarctica). Discoasteraceae include the genera Discoaster and Catinaster. Color coding represents the  
 1516 cluster assignment based on the nanofossil assemblage shown in fig. 4a.

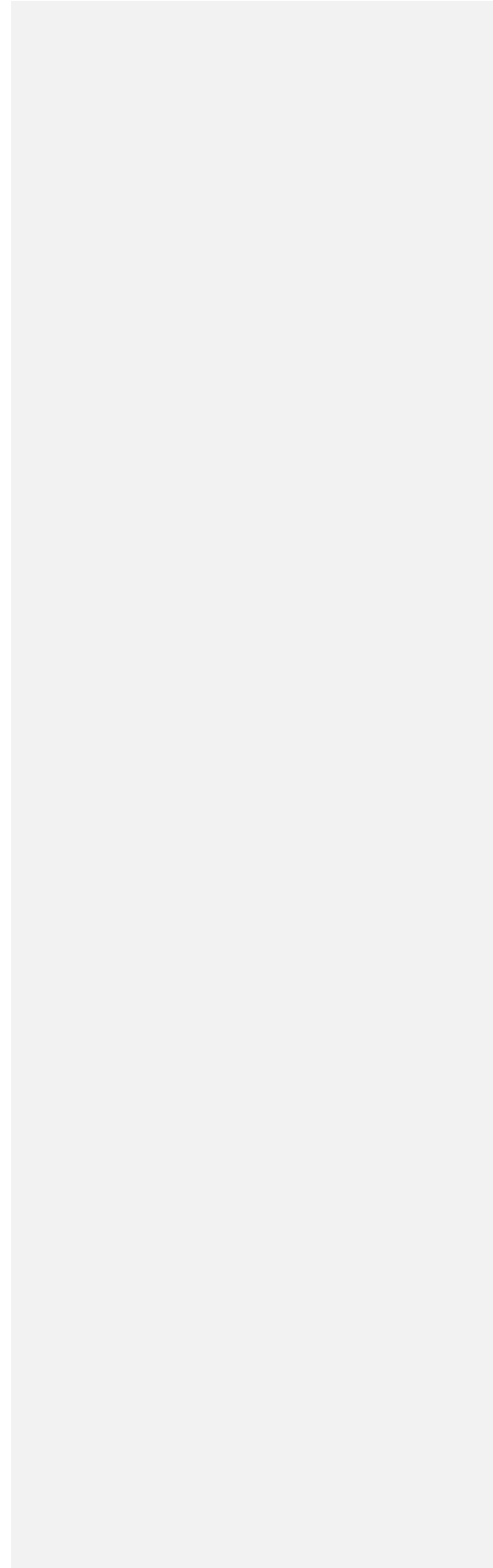
1517

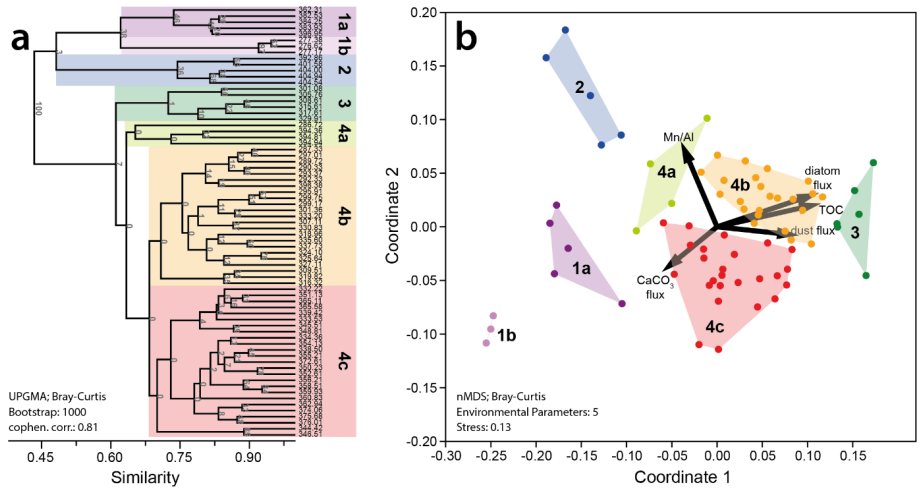


1518

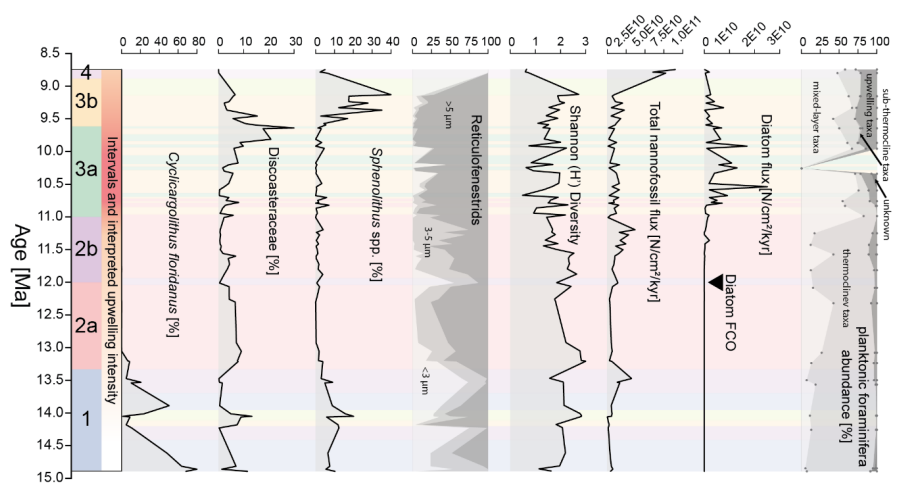
1519 **Figure 3:** Geochemical data initially published by Bialik et al. (2020a) as well as  $TEX_{86}^H$  based SST data of Zhuang et al.  
 1520 (2017). Data is shown in conjunction with the cluster analysis results based on the nanofossil assemblages, as shown in  
 1521 figure 4a. Total organic carbon (TOC in wt.%) is based on bulk sediment measurements. The Mn/Al ratio and the  
 1522 shown dust flux proxy, are based on benchtop XRF counts. Dust flux is calculated as  $\ln((Zr+Ti+Fe)/(Al+K))$  based on  
 1523 Kunt et al. (2015), with higher values indicating higher deposition of dust-born minerals at Site 722. Nitrogen isotopic  
 1524 data indicate increasing denitrification of sinking organic matter with higher values. On the left of the figure we also  
 1525 show intervals 1 – 4 and their respective sub-intervals a/b and the resulting interpreted upwelling intensity. All data is  
 1526 underpinned by the assigned clusters as defined in Figure 4.

1527





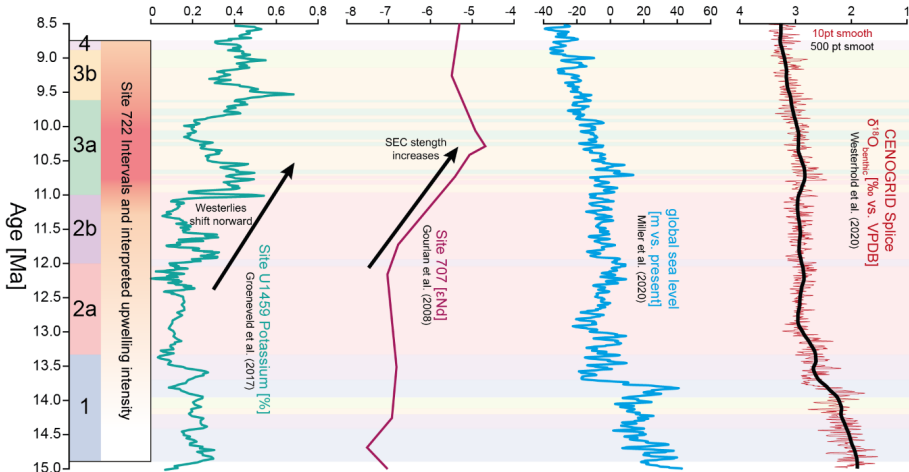
1529  
 1530 **Figure 4: Cluster analysis (a) and nMDS (b) based on the datasets shown in figs. 2 and 3. The geochemical data serves**  
 1531 **as paleoenvironmental proxies for high productivity (total organic carbon and siliceous fragments), high wind intensity**  
 1532 **(dust flux), water column oxygenation (Mn/Al), and high carbonate accumulation (CaCO<sub>3</sub> content/flux). Note the high**  
 1533 **correspondence of clusters 3 and, to some degree, 4b siliceous-fragment/diatom accumulation, dust flux, and high TOC**  
 1534 **content. They indicate that these clusters likely correspond to nannofossil assemblages thriving during intense**  
 1535 **upwelling. Conversely, lower productivity and, thus, higher water column oxygenation are marked by a correspondence**  
 1536 **of clusters 2 and 4a with higher Mn/Al values, denoting a less intense oxygen minimum zone.**



1538  
 1539 **Figure 5: Summary of relevant nannofossil taxa (C. floridanus, the sum of all Discoasteraceae, Sphenolithus spp.,**  
 1540 **as well as all 3 selected size ranges of Reticulofenestra spp.) shown as % abundance of the whole assemblage.**  
 1541 **Reticulofenestrads are combined into a single abundance graph showing the internal variability of the three defined size**  
 1542 **ranges of the genus Reticulofenestra. The Shannon (H') diversity is offered as an overall indicator of nanнопlankton**  
 1543 **diversity throughout the study interval. The total abundance of nannofossils fluxes in N/cm<sup>2</sup>/kyr illustrates the stark**  
 1544 **increase in nannofossil accumulation in interval 4, denoting the noted bloom in small reticulofenestrads after 8.8 Ma.**  
 1545 **Next, the nannofossil abundances are contrasted with diatom fluxes. The nannofossil assemblage variability is further**  
 1546 **shown with classical upwelling indicators based on planktonic foraminifera, which shows an overall constant abundance**  
 1547 **of upwelling indicative taxa (e.g., G. bulloides) between Interval 3a and 4, despite the dynamic changes in the**  
 1548 **phytoplankton data. On the left of the figure we also show intervals 1 – 4 and their respective sub-intervals a/b and the**  
 1549 **resulting interpreted upwelling intensity. All data is underpinned by the assigned clusters as defined in Figure 4. On the**

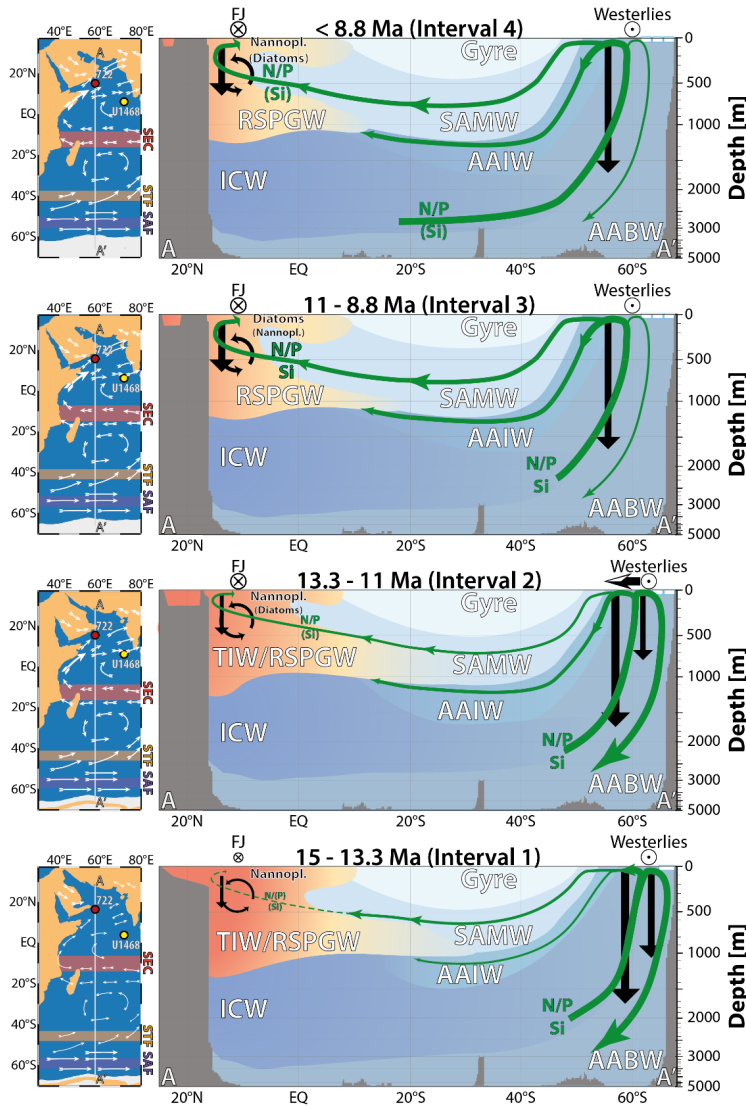
550 left of the figure we also show intervals 1—4 and their respective sub-intervals a/b, where applicable, all data is  
551 underpinned by the assigned clusters as defined in Figure 4.

**Formatted:** Font: Bold



1552 **Figure 6: Compilation of Indian Ocean and Global Data during the Study interval. Proposed plankton community**  
 1553 **intervals as well as nannofossil assemblages at Site 772 are presented next to the abundance of natural gamma radiation**  
 1554 **derived potassium content at Site U1459 (Groeneveld et al., 2017), interpreted to relate to precipitation changes in**  
 1555 **western Australia as a consequence of the northward shifting southern hemisphere westerlies. The εNd data of Gourlan**  
 1556 **et al. (2008), showing an increase in εNd signatures derived from Indonesia indicating an increase in SEC strength, due**  
 1557 **to a global increase in global ocean and atmospheric circulation (e.g., Betzler and Eberli, 2019). The global sea level**  
 1558 **reconstruction of Miller et al. (2020) showing stable sea levels after the MMCT until at least 11 Ma. The global stable**  
 1559 **CENOGRID stable oxygen isotope stack for the study interval, showing stable deep water conditions until 11 Ma**  
 1560 **(Westerhold et al., 2020). On the left of the figure we also show intervals 1–4 and their respective sub-intervals a/b and**  
 1561 **the resulting interpreted upwelling intensity. All data is underpinned by the assigned clusters as defined in Figure 4.**  
 1562

1552  
 1553  
 1554  
 1555  
 1556  
 1557  
 1558  
 1559  
 1560  
 1561  
 1562  
 1563



1565  
 1566 **Figure 7: Envisioned progression of upwelling along the Oman Margin based on paleogeography of Cao et al. (2017),**  
 1567 **adapted with regional information (Rögl, 1999; Bialik et al., 2019; Reuter et al., 2009, 2008), combined with**  
 1568 **hypothesized changing intermediate water-based nutrient supply throughout the study interval (c. 15 – 8.8 Ma). The**  
 1569 **figure also shows the hypothesized change in water masses over the study interval. Orange shading represents local**  
 1570 **water masses forming in the northern Arabian Ocean migrating southward. [While intermediate waters able to](#)**  
 1571 **[progressively migrate further in the the Arabian Sea where the begin to dominate upwelling by c. 11 Ma. Shading of](#)**  
 1572 **[the water masses represents their progressive intermixing with each other.](#)** Water masses shown are the Tethyan  
 1573 Intermediate Water (TIW), the Red Sea and Persian Gulf Intermediate Waters (RSPGW), Indian Central Water  
 1574 (ICW), southern Indian Ocean gyre waters (Gyre), sub-Antarctic mode water (SAMW), and the Antarctic intermediate  
 1575 water (AAIW) and Antarctic bottom waters (AABW). In addition, note the corresponding change in nutrient (N, P, and  
 1576 Si) transport – [visualized by green arrows](#) – following the proposed northward migration of the southern hemisphere  
 1577 westerlies due to sea ice expansion after 12 Ma (Groeneweld et al., 2017). Hypothesized changes in nutrient transport

1578 are based on model studies, which predict reduced low-latitude productivity during warmer climates (Laufkötter and  
 1579 Gruber, 2018; Moore et al., 2018). Black arrows indicate the changes in the fluxes and hypothesized recycling of organic  
 1580 matter within the WAS upwelling zone.

1581 **Table 1: Ecological interpretation of the defined nannofossil taphogroups based on the ecological parameters of the**  
 1582 **defining nannofossil taxa.**

| <i>Tapho-<br/>group</i> | <i>Defining Taxa</i>   | <i>Ecology</i>  | <i>References</i>  | <i>Environmental<br/>Parameters</i>  |
|-------------------------|--|---|--|--|
| <i>TG1a</i>             | <i>Reticulofenestra minuta</i> dominant  | Dominated by r-selected opportunistic nannofossil taxa. Commonly interpreted as nutrient elevation in the photic zone.                              | (Haq, 1980; Wade and Bown, 2006; Auer et al., 2015)  | Associated with high calcium carbonate accumulation  |
| <i>TG1b</i>             | Small and medium reticulofenestrids together with <i>Cyclicargolithus floridanus</i>                       | Warm to temperate waters, with increased nutrient conditions.   | (Wei and Wise, 1990; Wade and Bown, 2006; Auer et al., 2015)   | Associated with high calcium carbonate accumulation  |
| <i>TG2</i>              | <i>Cyclicargolithus floridanus</i> and common medium reticulofenestrids                                    | Warm to temperate waters, with moderate nutrient conditions.  | (Wei and Wise, 1990; Wade and Bown, 2006; Auer et al., 2015)   | Associated with high Mn/Al ratios (= weak OMZ) and elevated carbonate content                |
| <i>TG3</i>              | Large reticulofenestrids dominant with common Discoasterids  | Elevated nutrient conditions with deep nutricline and possible (seasonal) stratification  | (Lohmann and Carlson, 1981; Backman et al., 2013; Imai et al., 2015, 2017)   | Associated with biogenic silica, TOC, dust flux and lowered Mn/Al ratios (=stronger OMZ)     |
| <i>TG4a</i>             | Variable small, medium and large reticulofenestrids with common <i>Sphenolithus</i> spp. and discoasterids | Elevated nutrient conditions with high seasonal variability and intermittent stratification, possible indication of increased environmental stress. | (Castradori, 1998; Blanc-Valleron et al., 2002; Gibbs et al., 2004b; Wade and Bown, 2006; Villa et al., 2008; Beltran et al., 2014; Imai et al., 2015; Schueth and Bralower, 2015) | Weakly associated with carbonate accumulation and higher Mn/Al ratios (= weak OMZ)           |
| <i>TG4b</i>             | Large reticulofenestrids dominant  | High nutrient conditions, likely open marine and potentially stratified.  | (Auer et al., 2014, 2015; Beltran et al., 2014; Imai et al., 2017, 2015)   | Weakly associated with biogenic silica flux, TOC and reduced Mn/Al ratios (= increasing OMZ) |
| <i>TG4c</i>             | Medium and large reticulofenestrids dominant   | High nutrient levels, likely upwelling derived.   | (Haq and Lohmann, 1976; Lohmann and Carlson, 1981; Wade and Bown, 2006; Auer et al., 2014, 2019)   | Not associated with Mn/Al ratios (= strong OMZ), no strong association with other parameters |

1583



Table 2: Interpretation of habitat depth of the identified planktonic ~~foraminifer~~ **foraminifera** taxa.

| <i>Taxa</i>                           | <i>Habitat</i>             | <i>Reference</i>                                      | <i>Comments</i>   |
|---------------------------------------|----------------------------|---|---|
| <i>Dentoglobigerina altispira</i>     | open ocean mixed-layer     | (Berggren et al., 1985; Aze et al., 2011)             | Symbiont bearing  |
| <i>Fohsella fohsi</i>                 | open ocean thermocline     | (Aze et al., 2011)                                    |   |
| <i>Fohsella peripheronida</i>         | open ocean thermocline     | (Berggren et al., 1985; Aze et al., 2011)             | Extends to cool subtropical waters                                  |
| <i>Globigerina bulloides</i>          | upwelling                  | (Kroon et al., 1991)                                  |   |
| <i>Globigerina</i> sp.                | open ocean mixed-layer     | (Aze et al., 2011)                                    |   |
| <i>Globigerinita glutinata</i>        | open ocean mixed-layer     | (Majewski, 2003; Pearson and Wade, 2009)              |   |
| <i>Globigerinoides obliquus</i>       | open ocean mixed-layer     | (Nikolaev et al., 1998)                               |   |
| <i>Globigerinoides ruber</i>          | open ocean mixed-layer     | (Nikolaev et al., 1998)                               | Symbiont bearing  |
| <i>Globigerinoides</i> sp.            | open ocean mixed-layer     |   | Based on another present taxa of this genus                         |
| <i>Globoquadrina dehiscens</i>        | open ocean thermocline     | (Pearson and Shackleton, 1995; Nikolaev et al., 1998) | Noted to be erratic and variable by Pearson and Shackleton (1995).  |
| <i>Globorotalia archaemenardii</i>    | open ocean thermocline     |   | Based on similarities to <i>G. manardii</i>                         |
| <i>Globorotalia menardii</i>          | open ocean thermocline     | (Regenberg et al., 2010)                              |   |
| <i>Globorotalia plesiotumida</i>      | open ocean thermocline     | (Aze et al., 2011)                                    |   |
| <i>Globorotalia scitula</i>           | open ocean sub-thermocline | (Itou et al., 2001)                                   | <i>G. scitula</i> flux is inverse to POC flux                       |
| <i>Globorotalia</i> sp.               | open ocean thermocline     |   | Based on another present taxa of this genus                         |
| <i>Globorotaloides hexagonus</i>      | upwelling                  | (Spezzaferri, 1995)                                   | May also be deep sub-thermocline dweller (Brummer and Kučera, 2022) |
| <i>Globoturborotalita druryi</i>      | open ocean mixed-layer     | (Kennett and Srinivasan, 1983; Aze et al., 2011)      | Symbiont bearing  |
| <i>Globoturborotalita nepenthes</i>   | open ocean mixed-layer     | (Aze et al., 2011)                                    |   |
| <i>Neogloboquadrina acostaensis</i>   | open ocean thermocline     | (Aze et al., 2011)                                    |   |
| <i>Orbulina universa</i>              | open ocean mixed-layer     | (Aze et al., 2011)                                    |   |
| <i>Paragloborotalia mayeri</i>        | open ocean thermocline     | (Aze et al., 2011)                                    |   |
| <i>Sphaeroidinellopsis seminulina</i> | open ocean thermocline     | (Aze et al., 2011)                                    |   |
| <i>Sphaeroidinellopsis</i> sp.        | open ocean thermocline     | (Aze et al., 2011)                                    |   |
| <i>Trilobatus quadrilobatus</i>       | open ocean mixed-layer     | (Chaisson and Ravelo, 1997)                           | Deep mixed layer in Nikolaev et al. (1998)                          |
| <i>Trilobatus sacculifer</i>          | open ocean mixed-layer     | (Aze et al., 2011)                                    | Symbiont bearing  |
| <i>Trilobatus trilobus</i>            | open ocean mixed-layer     | (Aze et al., 2011)                                    | Symbiont bearing  |